

Iterative Maneuver Optimization in a Transverse Gust Encounter

Xianzhang Xu*

University at Buffalo, The State University of New York, Buffalo, New York 14260
Antonios Gementzopoulos,† Girguis Sedky,† and Anya R. Jones‡
University of Maryland, College Park, Maryland 20742

and

Francis D. Lagor§

University at Buffalo, The State University of New York, Buffalo, New York 14260

https://doi.org/10.2514/1.J062404

This paper presents a framework based on either iterative simulation or iterative experimentation for constructing an optimal, open-loop maneuver to regulate the aerodynamic force on a wing in the presence of a known flow disturbance. The authors refer to the method as iterative maneuver optimization and apply it in this paper to regulate lift on a pitching wing during a transverse gust encounter. A candidate maneuver is created by performing an optimal control calculation on a surrogate model of the wing–gust interaction. Execution of the proposed maneuver in a high-fidelity simulation or experiment provides an error signal based on the difference between the force predicted by the surrogate model and the measured force. The error signal provides an update to the reference signal used by the surrogate model for tracking. A new candidate maneuver is calculated such that the surrogate model tracks the reference force signal, and the process repeats until the maneuver adequately regulates the force. The framework for iterative maneuver optimization is tested on a discrete vortex model as well as in experiments in a water towing tank. Experimental results show that the proposed framework generates a maneuver that reduces the magnitude of lift overshoot by 92% for a trapezoidal gust with peak velocity equal to approximately 0.7 times the freestream flow speed.

		Nomenclature	LESPc	=	critical value of leading-edge suction param-
a	=	pitch-axis location in semichords			eter
b	=	semichord length, $c/2$	m_1, m_2	=	functions defining bounding curves in C_L
C_i	=	fitting parameter in the modified Goman-			versus angle-of-attack plane
		Khrabrov model	p	=	number of specified states at terminal time of
C_L	=	lift coefficient			optimal-control problem
$C_{L,\mathrm{model}}$	=	lift coefficient predicted by the modified	q	=	internal variable in the Goman–Khrabrov lift model
		Goman-Khrabrov model	~		
$C_{L,\mathrm{ref}}$	=	reference value for lift coefficient	q_0	=	empirical function in the Goman–Khrabrov
$C_{L,\mathrm{test}}$	=	lift coefficient measured in experiment or	_		lift model
		high-fidelity simulation	$q_{ m ref}$	=	q value corresponding to $C_{L,\text{ref}}$
c	=	chord length	R	=	matrix of influence costates for terminal con-
f	=	dynamics function in optimal-control algo-			straint sensitivity in optimal-control algo-
		rithm			rithm
GR	=	gust ratio, $V_{\rm max}/\overline{V}$		=	surge rate
H	=	Hamiltonian in optimal-control theory	t^*	=	convective time, Ut/c
\dot{h}	=	plunge rate	t_0, t_f	=	start time and terminal time of optimal-
$I_{\psi\psi},I_{\psi\mathrm{J}},I_{\mathrm{J}\psi},I_{\mathrm{J}\mathrm{J}}$	=	integral terms in optimal control algorithm			control problem
I	=	performance measure for optimal control	и	=	control input signal
Ĩ	=	performance measure augmented with termi-	u_0	=	initial guess of control input signal in
J		nal constraints			optimal-control algorithm
ĵ	=	modified performance measure in the itera-	(u',v')	=	components of flow-relative velocity
J		tive maneuver optimization method	(u_x, u_z)	=	external flow components in the inertial
K	=	proportional feedback control gain			reference frame
L	=	Lagrangian function in optimal-control theory	\overline{V}	=	constant, characteristic flow speed
			$V_{\rm max}$	=	maximum velocity of gust
			V_{∞}	=	speed of freestream flow
			W	=	gust width
Presented as Pap	21-2937 at the AIAA Aviation 2021 Forum, Virtual	x	=	state vector	
Event, August 2-6,	1; received 2 September 2022; revision received 28	X c	=	reference state vector	

Presented as Paper 2021-2937 at the AIAA Aviation 2021 Forum, Virtual Event, August 2–6, 2021; received 2 September 2022; revision received 28 December 2022; accepted for publication 3 January 2023; published online 31 January 2023. Copyright © 2023 by the American Institute of Aeronautics and Astronautics, Inc. All rights reserved. All requests for copying and permission to reprint should be submitted to CCC at www.copyright.com; employ the eISSN 1533-385X to initiate your request. See also AIAA Rights and Permissions www.aiaa.org/randp.

*Graduate Student, Department of Mechanical and Aerospace Engineering. Student Member AIAA.

[†]Graduate Research Assistant, Department of Aerospace Engineering. Student Member AIAA.

[‡]Professor, Department of Aerospace Engineering. Associate Fellow AIAA. [§]Assistant Professor, Department of Mechanical and Aerospace Engineering. Senior Member AIAA.

attack and pitch rate

θ_0	=	angular coordinate of evaluation location on
		mean camber line
λ	=	costate vector
ν	=	Lagrange multiplier vector
Ξ	=	positive-definite weight matrix in optimal control algorithm
τ_1, τ_2	=	time constants in Goman-Khrabrov lift model
Ψ	=	terminal constraint function

I. Introduction

IND gusts and other unsteady flowfields can create significant aerodynamic disturbances for small aircraft such as micro-air vehicles, which are vulnerable to large-amplitude gusts due to their relatively small size and slow speed [1]. Modeling large-amplitude gust encounters is challenging, because massive flow separation and shed vorticity create nonlinear effects in the force response of the vehicle [2]. Gust interactions become even more complex with the inclusion of wing motion during the encounter. To better understand this threat to small aircraft, aerodynamic modeling [2–7] and control [8–11] in unsteady flowfields at low Reynolds numbers have become very active areas of research.

Researchers have taken various approaches to model largeamplitude gust encounters. Some works [2,3,7,12,13] have examined classical thin-airfoil models based on an attached-flow assumption to determine the extent of their applicability. Quasi-steady thin-airfoil theory can model slowly varying airfoil behaviors in pitch, plunge, and surge [14], and a gust flowfield can be included in the quasisteady theory through the use of effective angle of attack [4,15]. Unsteady thin-airfoil theory developed by Wagner, Theodorsen, Küssner, and von Kármán [16-19] can provide linear models of the wing's response to the gust that also include acceleration terms and wake effects. These quasi-steady and unsteady models provide some predictive power as noted in the findings of high-fidelity numerical simulations [12,13,20] and experimental studies [2,3]. However, these findings are limited to the strengths, widths, and shapes of the gusts examined in these works. Küssner's theory deviates significantly from experimental and numerical results for large-amplitude gusts and sharp-edge (e.g., top-hat) gusts [12]. Moushegian et al. [12] showed in delayed detached eddy simulation (DDES) that the lift response deviates appreciably from Küssner's theory if the gust ratio, which is the ratio of the maximum gust velocity to the freestream velocity, exceeds 0.5.

Deviation of the force response from linear theory can be attributed to the breakdown of the attached-flow assumption and the role of shed vorticity in the flowfield. Perrotta and Jones [21] and Grubb et al. [13] showed that linear, thin-airfoil theories fail to closely model the lift response when flow separation occurs before the wing enters the gust region. Previous works [2,3,13,20] determined that the leading-edge vortex (LEV) plays an important role in the force response of the wing during the gust encounter. LEV formation and separation also affect the time at which the maximum force occurs [22]. To capture the role of shed vorticity in the lift response, discrete vortex models (DVMs) have been used extensively to produce flowfields that closely agree with higher-fidelity numerical simulations and experiments for problems such as LEV formation, dynamic stall, and kinematic motion at high angles of attack [23–25]. Recent research works [7,26-28] have employed DVM methods to model gust disturbances for the purposes of flow sensing, estimation, and flow interaction. The current paper uses a DVM to evaluate the performance of lift-regulating maneuvers.

Mitigation of transient forces in a gust encounter through maneuvering is currently being studied from both open-loop (i.e., predetermined) and closed-loop (i.e., calculated based on real-time sensor measurements) perspectives. To examine how control actuation influences lift during a gust encounter, Sedky et al. [4] used a model-based feedback controller with an observer to reduce the transient lift response for a pitching wing. Closed-loop simulations were performed to design maneuvers that were executed in open-loop experiments. The study in [7] deconstructed the force contributions to

lift that occurred using a (model-free) proportional feedback control in closed-loop DVM simulation of a gust encounter. In open-loop maneuvers, Andreu-Angulo and Babinsky [6] examined different pitch profiles for a flat plate encountering a top-hat gust and broke down the force response into contributions from gust vorticity, wing motion, and shed vorticity. Both works [4,6] found that vortex shedding was a key contribution to the lift overshoot experienced by a nonmaneuvering wing and that the added-mass force can be used to negate most of the lift overshoot through pitching of the wing. Andreu-Angulo and Babinsky [5] proposed an analytical model based on theories of Wagner and Küssner to calculate an ideal pitch profile for maintaining zero lift during an encounter with a top-hat gust. Although the approaches differ, each of works [4–6] seeks an optimal maneuver for force regulation or a controller to generate these maneuvers.

An optimal maneuver should ideally regulate the aerodynamic force during the encounter. Optimal maneuvers are important because they can show how to best achieve rejection of the gust force through regulation of coherent structure formation, interaction with coherent structures, and management of the sources of aerodynamic force contributions (e.g., added-mass and circulatory contributions). Previous works in [29,30] also studied generation of optimal pitch maneuvers of a wing. Milano and Gharib [29] employed a genetic algorithm to evolve a pitch maneuver in experiments in order to maximize the average lift force produced. They established a connection between maximizing the force on the wing and maximizing the circulation strength of the LEV. Peng and Milano [30] further identified a range of key parameters associated with the optimal lift trajectories through similar experimental measurements. These works demonstrated how iterated experiments can optimize an aerodynamic force objective and be used to study the physical mechanisms involved in force production. Systematic optimization through iterated experiments has not yet been applied to gust encounters. The current paper changes the aerodynamic objective from lift maximization to lift regulation. Additionally, the current paper differs from these prior works based on the algorithm used to perform the optimization. The genetic algorithm utilized by Milano and Gharib [29] required approximately 3000 experiments to achieve an optimized maneuver. The method developed in the current paper utilizes a model of the wing-gust encounter to guide maneuver updates, which enables construction of the optimal maneuver in approximately 10 or fewer experiments. Even though each experiment consists of several runs of the same maneuver, the proposed method significantly reduces overall experimental effort.

To guide a maneuver update, this paper examines the calculation of an optimal maneuver in a prescribed flowfield using an algorithm from optimal control theory. The algorithm requires a dynamic model of the wing-gust interaction. A Goman-Khrabrov (GK) model is a low-order, dynamic model that can predict the unsteady lift force. Several recent studies [31–33] have used a GK model for control design. For example, Williams and King [33] developed a closedloop controller based on a modified GK model that can alleviate gust loading during periodic pitching through the use of jet actuators. This paper uses a modified Goman-Khrabrov (mGK) model that includes effective angle of attack to incorporate wing kinematics and the external flow disturbance of the gust. The optimal control formulation integrates a quadratic cost for lift deviations over a fixed-time interval, subject to the dynamics of the mGK model and terminal constraints on pitch angle and pitch rate. In preliminary work [34], the authors applied the proposed optimal control framework to regulate the lift during encounters with ideal, sine-squared gusts. However, the optimal maneuver calculated in this manner is only optimal subject to the accuracy of wing-gust interaction model. Unmodeled effects cause lift deviations when an optimized control profile is applied in experiments. Constructing a truly optimal maneuver in a transverse gust encounter requires optimization over experimental data.

The objective of this paper is to provide researchers with a tool to generate optimized maneuvers for further study of flow interactions. This paper constructs an optimal maneuver for a real flowfield by iteratively updating the maneuver to account for unmodeled effects that result in regulation errors during experiments. This approach is an extension of the work of Andreu-Angulo and Babinsky [6], which constructed a hybrid maneuver by updating a model-proposed maneuver based on the lift error signal from experiment. This paper proposes a framework that the authors refer to as iterative maneuver optimization (IMO). IMO performs an optimal control calculation over a surrogate model of the system, which is a low-order model that is inexpensive to evaluate [35]. The mGK model serves as the surrogate model in the proposed IMO framework, although other surrogate models are possible. An optimal control calculation generates a candidate maneuver that regulates the force to a desired reference value. Then, IMO tests the proposed control signal in an experiment or a higher-fidelity simulation. The actual force signal is compared to the predicted force from the surrogate model, and the error is used to update the reference signal that the surrogate model tracks, and the process repeats, and lift regulation generally improves with each iteration. Numerical simulations in this paper suggest that a proportional output-feedback controller with high feedback gain can generate the optimal control profile for the mGK model. Since the proportional output-feedback control is computationally cheaper than the optimal control method, this paper recommends outputfeedback simulations for optimization of the mGK model at each

The proposed IMO method is similar to iterative learning control (ILC) in the control-system literature. ILC seeks an input to an unknown or uncertain system that makes the output of the system nearly identical to a desired output [36]. These methods both use measurement data to update and refine the control input to improve the controlled behavior of the uncertain system. However, there are some differences between IMO and ILC related to the control profile update. Most ILC architectures apply a learning function to the error signal or its time rate of change to update the previous control sequence. In contrast, each iteration of IMO performs an optimal-control calculation in place of the learning function to generate a new proposed control signal. Iterative feedback tuning (IFT) is another iterative method that optimizes a control input based on experimental data [37]. However, this method tunes the gains of a controller based on the output error signal, rather than seeking a prescribed input.

This paper contributes an optimal control framework for minimizing the lift response during a wing-gust encounter based on a modified GK model. This paper also contributes an IMO method that can rapidly optimize a pitch maneuver through repeated experiments. The proposed method applies to transverse gusts but may also be applicable to other steady-flow disturbances. This method does not require a highly accurate model to capture the physics of the flowfield, because good performance can be achieved by refinement through iteration. These contributions are important because the framework can make use of an imperfect model to generate optimal

maneuvers for a real flowfield through iterative experimentation or high-fidelity simulation.

The outline of this paper is as follows. Section II presents background information on effective angle of attack and a modified GK model of a gust encounter. The experimental setup is introduced to collect training data for the mGK model. Section III formulates the optimal-control problem for a gust encounter, presents simulation results for a trapezoidal gust, and compares the optimal control to proportional output-feedback control. Section IV proposes the IMO method to construct an optimal pitch maneuver in experiment (or high-fidelity simulation) and tests the framework in a DVM simulation. Section V presents and analyzes the results of water towing tank experiments. Section VI concludes the paper and discusses directions for future investigation.

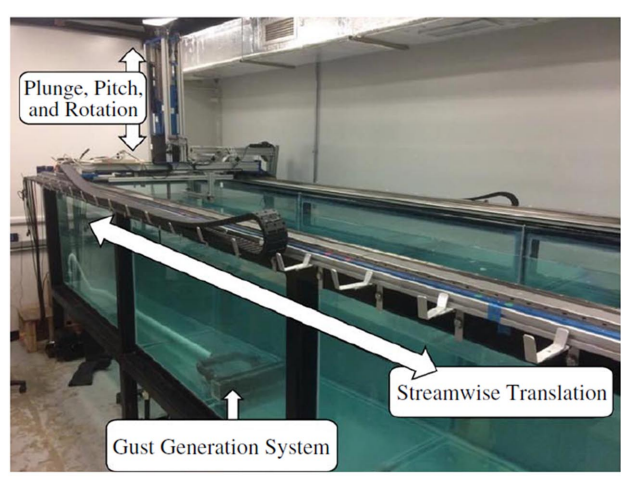
II. Gust Encounter Modeling

This section develops an empirical model of a wing–gust encounter based on experimental data collected in a towing tank setup with a built-in gust generator. This section first introduces the experimental setup that is used. Next, this section modifies a GK model for a rapidly pitching wing to incorporate a prescribed gust flowfield. The resulting mGK model is put in state-space form for the optimal control framework in Sec. III.

A. Experimental Setup

The GK model requires experimental measurements to fit its empirical terms. Experiments were carried out in a free-surface water towing tank at the University of Maryland (UMD). The tank is 7 m long, 1.5 m wide, and 1 m deep, as shown in Fig. 1a. The tank is equipped with a four-degree-of-freedom motion-control system, allowing for surging, pitching, and plunging motions of a wing model. The freestream is created by towing the wing through the tank, and a transverse gust is created using a recirculating jet driven by a variable speed 1.85 HP Hayward centrifugal pump. Details on the gust design and profile can be found in [38].

The wing model used in the experiments has a NACA 0012 profile with a chord of 0.102 m and a span of 0.254 m, as shown in Fig. 1b. The wing is isolated from flow disturbances that may be created by the pitching mechanism or force balance through the use of a circular, stainless-steel splitter plate. The pitching mechanism and splitter plate are located in the approximate center of the tow tank's cross-stream direction. Although the wing's aspect ratio is 2.5, the splitter plate creates an effective aspect ratio of 5. On the opposite end of the wing, the wing tip is free and away from the wall of the tank. The wing was manufactured using a Formlabs Fuse 1 3D printer. The wing was then treated using waterproof spray paint to reduce warping due to water absorption. The wing pitches about its center of gravity (42% of the chord from the leading edge) and is



a) Towing tank at the university of maryland



b) NACA 0012 wing on a pitching mechanism

Fig. 1 Experimental apparatus at the University of Maryland water towing tank.

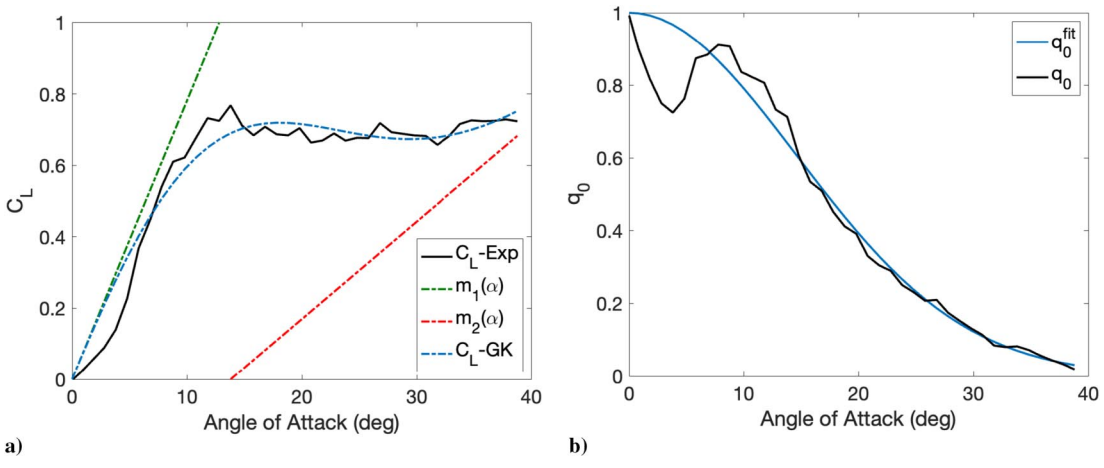


Fig. 2 a) Steady C_L versus α curve for a NACA 0012 finite wing with bounding curves m_1 and m_2 . b) Empirical function q_0 versus α and a Gaussian curve fit.

attached to a six-degree-of-freedom ATI Mini-40 force balance that measures forces and moments at 1 kHz. The force measurements were filtered by a zero-lag, low-pass Butterworth filter with a cutoff frequency of 5 Hz. Each experiment (i.e., iteration of the IMO method) was repeated five times and force measurements were ensemble averaged over the five runs. The experiments were conducted at Reynolds number 12,000.

B. Goman-Khrabrov Lift Model

Goman and Khrabrov [39] developed a low-order, empirical modeling approach for unsteady aerodynamic forces and moments without an attached-flow assumption [31,40]. A GK model for lift consists of an internal variable that represents the degree of flow attachment, an empirical function for the steady-state values of the internal variable for varying angles of attack, and first-order dynamics that model the return to steady-state conditions after perturbation. With two time constants and an empirical steady-state function, a GK model is capable of fitting a variety of aerodynamic force behaviors. In addition, the low-order form of the dynamics enables rapid simulation, which is an important consideration in the optimal-control framework presented in this paper.

Let q be an internal variable that describes the degree of flow attachment and let C_L be the dimensionless lift coefficient [40]. For a wing with angle of attack α and pitch rate $\dot{\alpha}$, the GK lift model is [41]

$$\tau_1 \dot{q} + q = q_0 (\alpha - \tau_2 \dot{\alpha}) \tag{1}$$

$$C_L = m_1(\alpha)q + m_2(\alpha)(1-q)$$
 (2)

where $q_0(\cdot)$ is an empirical function obtained from steady-state values of q for various angles of attack, and $m_1(\cdot)$ and $m_2(\cdot)$ are empirical functions of α that bound the lift curve and its variations in time in the C_L versus α plane. When the angle of attack increases from low to high, the value of q varies from approximately 1, representing fully attached flow, to 0, representing fully separated flow. Time constant τ_1 indicates the time for separated flow to reach steady state, and time constant τ_2 relates to the time-rate of change in angle of attack. Researchers (e.g., see [31,32,41]) commonly choose m_1 and m_2 to be linear fits of the steady C_L versus α curve in the attached and separated flow regions, respectively. Occasionally, these choices for m_1 and m_2 do not enclose the data in a convex region of the plane because the lift curve deviates from an ideal shape (e.g., see [4]). Figure 2a shows steady lift data for a NACA 0012 wing that is used in the experiments of Sec. V. Note that the lift slope for $\alpha < 5$ deg is less than the slope for $5 \le \alpha \le 10$ deg. This change in slope indicates the presence of a separation bubble that often occurs for a NACA 0012 wing operating at a low Reynolds number [42]. Also note that the separated slope in the region $\alpha \ge 25$ deg is small, and a linear fit in this region would lead to an m_2 line that intersects rather than bounds the remainder of the lift curve. Given the data in Fig. 2a, this paper does not use m_1 and m_2 to represent fits of the attached and separated portions of the curve. Instead, m_1 and m_2 are only required to enclose the data in a convex region of the plane. An et al. [43] choose

$$m_1(\alpha) = C_1(\alpha - C_3)$$
 and $m_2(\alpha) = C_2(\alpha - C_4)$ (3)

where C_1 and C_2 are the attached and separated lift slopes, C_3 is the zero-lift angle, and $C_2(\alpha - C_4)$ is the C_L value at the smallest angle when the flow is fully separated. A fitting procedure detailed in the following discussion determines the constants C_1 , C_2 , C_3 , and C_4 concurrently with a fit of the q_0 function.

Optimal trajectory calculations in Sec. III make use of a q_0 function that is replaced by a Gaussian fit as shown in Fig. 2b. Often, researchers who use GK models query the q_0 curve directly and perform data interpolation. Fitting a Gaussian to the $q_0(\alpha)$ curve is a useful approximation that improves the efficiency for the optimal-control calculations in Sec. III. A Gaussian fit is justified because the IMO method of Sec. IV only requires an approximate fit for the GK model. An optimization procedure can find all the coefficients in the m_1, m_2 , and q_0 curves that best fit the experimental steady-lift data in Fig. 2a. The Gaussian fit of the q_0 curve and the m_1 and m_2 lines are adjusted by the optimization problem

$$\begin{split} \min_{C_0,C_1,C_2,C_3,C_4} & \frac{1}{2} \sum_{k}^{N} \left(C_L^{(\text{exp})}(\alpha_k) - C_L^{(\text{GK})}(\alpha_k) \right)^2 \\ \text{subject to} & C_L^{(\text{GK})}(\alpha) = C_1(\alpha - C_3) q_0^{(\text{fit})} + C_2(\alpha - C_4) (1 - q_0^{(\text{fit})}) \\ & q_0^{(\text{fit})}(\alpha) = \exp \left(\frac{-\alpha^2}{C_0} \right) \end{split}$$

$$(4)$$

where $q_0^{(\mathrm{fit})}$ is the Gaussian fit, $C_L^{(\mathrm{GK})}(\alpha)$ is the steady GK lift model, and $C_L^{(\mathrm{exp})}(\alpha)$ is the steady experimental data at discrete angles of attack α_k for $k=1,\ldots,N$. This problem can be numerically solved using existing optimization functions in MATLAB. Figure 2a shows the results of fitting the steady parameters C_1,C_2,C_3 , and C_4 in a GK model. Figure 2b shows the result of fitting the C_0 parameter to approximate the $q_0(\alpha)$ curve with a Gaussian. The remaining parameters in a GK model are the time constants τ_1 and τ_2 that require fitting the model to an unsteady dataset. Section II.D performs the dynamic fit to obtain τ_1 and τ_2 parameters for the wing used in the experiments of this paper.

C. Effective Angle of Attack

Effective angle of attack is a composite quantity that integrates effects from an external flowfield with effects from kinematic motions such as pitching, plunging, and surging. Several works [44–46] have used quantities similar to effective angle of attack in

construction of state-space models that predict the unsteady lift response of an actuated wing. For a thin airfoil of semichord b pitching and plunging in a freestream with speed V_{∞} , the classical quasi-steady effective angle of attack is [14]

$$\alpha_{\rm eff} = \alpha + \frac{\dot{h}}{V_{\infty}} + b \left(\frac{1}{2} - a\right) \frac{\dot{\alpha}}{V_{\infty}} \tag{5}$$

where \dot{h} is the plunge rate, $\dot{\alpha}$ is the pitch rate, and a locates the pitch axis along the chord. In [15], the authors present a more general effective angle-of-attack expression

$$\alpha_{\text{eff}} = -\frac{1}{\pi} \int_0^{\pi} \frac{w' - u' \frac{dz}{dx}}{\overline{V} \sqrt{1 + \left(\frac{dz}{dx}\right)^2}} (\cos \theta_0 - 1) \, \mathrm{d}\theta_0 \tag{6}$$

that incorporates the external flow effects by integrating the local flow velocity along the chord, where \overline{V} is a characteristic flow speed, which is often set to the freestream flow speed V_{∞} , and θ_0 is a coordinate that parameterizes the airfoil chord from $\theta_0=0$ at the leading edge to $\theta_0=\pi$ at the trailing edge. Effective-angle-of-attack expression (5) also contains the camber slope dz/dx so that it is also applicable for cambered airfoils. In [15], the authors show that, for a maneuvering symmetric airfoil in uniform flow, the expression of effective angle of attack (6) properly encompasses the classical quasisteady effective angle of attack in Eq. (5). The relative velocity components at location θ_0 are

$$u'(\theta_0) = (\dot{s} - u_x)\cos\theta_g - (\dot{h} - u_z)\sin\theta_g - \dot{\theta}_g(z(\theta_0) - z_C)$$
 (7)

$$w'(\theta_0) = (\dot{s} - u_x)\sin\theta_g + (\dot{h} - u_z)\cos\theta_g + \dot{\theta}_g \left(\frac{c}{2}(1 - \cos\theta_0) - x_C\right)$$
(8)

which include the external flow components u_x and u_z , and surging, pitching, and plunging terms, \dot{s} , $\dot{\theta}_g$, and \dot{h} , respectively. Here, θ_g is the geometric angle of attack of the airfoil (i.e., the pitch angle). The notation for the angle of attack α is replaced in this paper by θ_g to highlight that θ_g represents only the orientation angle of the wing; the local angle of the external flow enters from the (u_x, u_z) flow components in $\alpha_{\rm eff}$. The coordinates of the pitch-axis center in the airfoil's body frame are (x_C, z_C) . Note that the derivation of Eqs. (6–8) in [15] uses a coordinate system in which the body-z direction is positive downward in agreement with a convention in aircraft flight dynamics.

In subsequent sections, this paper considers a pitching symmetric airfoil. For this scenario, the effective angle of attack simplifies to

$$\alpha_{\text{eff}} = -\frac{\dot{s}}{\overline{V}}\sin\theta_g + \frac{\dot{\theta}_g}{\overline{V}} \left(\frac{3}{4}c + x_C \right) + \frac{\cos\theta_g}{\pi\overline{V}} \int_0^{\pi} u_z(\theta_0)(\cos\theta_0 - 1) \,d\theta_0$$
 (9)

In the modified GK model, the rate of change of effective angle of attack can be derived by differentiating Eq. (9) with respect to time, yielding

$$\dot{\alpha}_{\text{eff}} = -\frac{\dot{s}\dot{\theta}_g}{\bar{V}}\cos\theta_g + \frac{\ddot{\theta}_g}{\bar{V}}\left(\frac{3}{4}c + x_C\right) + \frac{1}{\pi} \int_0^{\pi} \frac{u_z(\theta_0)\dot{\theta}_g\sin\theta_g - \dot{u}_z(\theta_0)\cos\theta_g}{\bar{V}}(\cos\theta_0 - 1)\,\mathrm{d}\theta_0 \qquad (10)$$

Note that the surge rate \dot{s} is constant in this paper, and the pitch acceleration $\ddot{\theta}_g$ appears in the equation. The pitch acceleration serves as the control variable in Sec. III.

D. Modified Goman-Khrabrov Model for Gust Encounters

This section introduces the mGK model used in this paper. The model incorporates the effective angle of attack to predict the lift force experienced while maneuvering in a transverse gust encounter. Previous work [4] presented a modified GK model that allows for incorporation of a gust by replacing the geometric angle of attack and the pitch rate in Eqs. (1) and (2) by the effective angle of attack and its rate of change, respectively. Additionally, a term is included in [4] to model the added-mass effect, which is important for rapid maneuvers. Added mass describes the inertial resistance of fluid surrounding the body during acceleration of the body [47]. The added-mass force required to accelerate this inertia can greatly influence the lift for a maneuvering wing. Even though a GK model is an empirical dynamic model that can be fit to force data, it is shown in [4] that explicitly including a separate term for added mass in the output equation can improve the model's fit. Stutz et al. [48] also noted a deficiency in the GK model due to a lack of an addedmass term.

The modified GK model used in this paper (hereafter, the mGK model) is

$$\dot{q} = \frac{1}{\tau_1} (-q + q_0(\alpha_{\text{eff}}(\theta_g, \dot{\theta}_g) - \tau_2 \dot{\alpha}_{\text{eff}}(\theta_g, \dot{\theta}_g, \ddot{\theta}_g)))
C_L = C_1(\alpha_{\text{eff}}(\theta_g, \dot{\theta}) - C_3)q + C_2(\alpha_{\text{eff}}(\theta_g, \dot{\theta}_g) - C_4)(1 - q)
+ C_5 \left(\dot{\theta}_g - \frac{ab}{\overline{V}} \ddot{\theta}_g\right)$$
(11)

Equation (11) incorporates the gust velocity through the effective angle of attack. The effective angle of attack in Eq. (9) is a function of θ_g and $\dot{\theta}_g$, and the time derivative of effective angle of attack (10) is a function of θ_g , $\dot{\theta}_g$, and $\ddot{\theta}_g$. The explicit $\dot{\theta}_g$ and $\ddot{\theta}_g$ terms in the C_L output equation are added-mass terms based on Theodorsen's expression for added mass [16]. Instead of using Theodorsen's analytical expression, the constant term $\pi b/\overline{V}$ is replaced by the empirical coefficient C_5 , which can be trained to improve the model fit for a maneuvering wing. After the steady fit in Sec. II.B is complete, the additional coefficient C_5 can be derived simultaneously with time constants τ_1 and τ_2 . In this work, the τ_1 and τ_2 parameters are trained to match the lift coefficient of a periodic pitching wing without the presence of a gust. The reduced frequency for a gust encounter is $k = \pi c/(2W)$, where c is the chord length of the wing and W is the gust width [7]. The maneuver for training data was set to periodically pitch at reduced frequency k = 1, which is approximately the reduced frequency of the gust in this work. The dynamic-fit procedure for parameters C_5 , τ_1 , and τ_2 of the mGK model involves solving the optimization problem

$$\begin{split} \min_{C_5,\tau_1,\tau_2} & \frac{1}{2} \sum_{k}^{N_t} (C_L^{(\text{exp})}(\alpha_k) - C_L^{(\text{GK})}(\alpha_k)) \\ \text{subject to} & C_L^{(\text{GK})}(\alpha) = C_1(\alpha - C_3) q_0^{(\text{fit})} + C_2(\alpha - C_4) (1 - q_0^{(\text{fit})}) \\ & + C_5 \Big(\dot{\theta}_g - \frac{ab}{\overline{V}} \ddot{\theta}_g \Big) \\ q_0^{(\text{fit})} &= \exp \bigg(\frac{-\alpha^2}{C_0} \bigg) \end{split} \tag{12}$$

Similar to the steady fit, this problem can be solved using MAT-LAB's optimization functions to find the dynamic fit variables C_5 , τ_1 , and τ_2 .

Figures 3a and 3b present the lift coefficients measured from experiment (black lines) and predicted by the mGK model (red lines) for sinusoidal pitching between -40 and 40 deg with reduced frequency k=1. The results show that the trained τ_1 and τ_2 values fit both the phase and amplitude of the lift coefficient well for the prescribed pitching motion of the wing. The resulting parameter values were $(C_5, \tau_1, \tau_2) = (0.531, 0.287, 0.165)$, where τ_1 and τ_2 are nondimensionalized by c/\overline{V} .

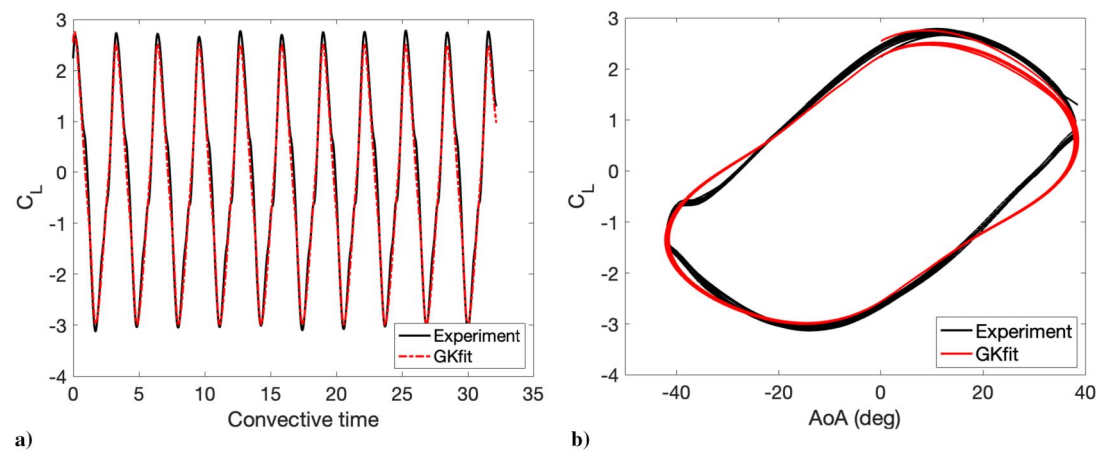


Fig. 3 Measured lift coefficients compared to the mGK model for a sinusoidal pitching motion with k = 1.

The optimal-control framework in Sec. III requires the system's dynamics to be in state-space form. Let the state vector be

$$\mathbf{x} = \begin{bmatrix} x_1 \\ x_2 \\ x_3 \end{bmatrix} \begin{bmatrix} \theta_g \\ \dot{\theta}_g \\ q \end{bmatrix} \tag{13}$$

and the output be

$$y = C_L(\alpha_{\text{eff}}(\theta_g, \dot{\theta}_g), q, \ddot{\theta}_g)$$

For a pitch acceleration input, such that $\ddot{\theta}_g = u$, the mGK model (11) in state-space form is

$$\begin{bmatrix} \dot{x}_{1} \\ \dot{x}_{2} \\ \dot{x}_{3} \end{bmatrix} = \begin{bmatrix} x_{2} \\ u \\ \frac{1}{\tau_{1}} (-x_{1} + q_{0}^{\text{fit}}(\alpha_{\text{eff}}(x_{2}, x_{3}) - \tau_{2}\dot{\alpha}_{\text{eff}}(x_{2}, x_{3}, u))) \end{bmatrix},$$

$$y = C_{1}(\alpha_{\text{eff}}(x_{2}, x_{3}) - C_{3})x_{3} + C_{2}(\alpha_{\text{eff}}(x_{2}, x_{3}) - C_{4})(1 - x_{3}) + C_{5}\left(x_{2} - \frac{ab}{\overline{V}}u\right)$$

$$(14)$$

State-space form (14) differs from the form given in [4] because the state variables in [4] are error states relative to a reference flight condition. Additionally, the effective angle of attack $\alpha_{\rm eff}$ is not treated as a state variable in Eq. (14) since it is a known function of the other states. The functions $\alpha_{\rm eff}(\cdot)$ and $\dot{\alpha}_{\rm eff}(\cdot)$ are retained in Eq. (14) for notational brevity. The order of the variables in the state vector also differs from [4], because the state-space form (14) is designed for the gradient-descent algorithm in the optimal-control framework of Sec. III. The algorithm requires variables that are treated as unconstrained at the terminal time to be listed last in the state vector. This paper does not constrain q at the terminal time, so it appears last in the state vector.

Figure 4 shows the time-averaged velocity profile of a trapezoidal gust (gray line) that has a gust ratio of approximately 0.7 and a gust width of approximately 1.5c. The velocity data of the trapezoidal gust were measured using particle image velocimetry (PIV) in [38]. The black line shows the lift coefficient measured during the gust encounter for a nonmaneuvering wing traveling at a constant speed of 0.118 m/s, corresponding to a Reynolds number of 12,000. Note that the simulation of the mGK model (red line) approximately captures the magnitude of the lift overshoot during the encounter. However, there is a noticeable delay in the mGK simulated response compared to the lift measured in experiment. This delay for a modified GK model is also noted and discussed by the authors in previous work [34] for a sine-squared gust and may be attributable to the role of leading-edge shed vorticity, which is

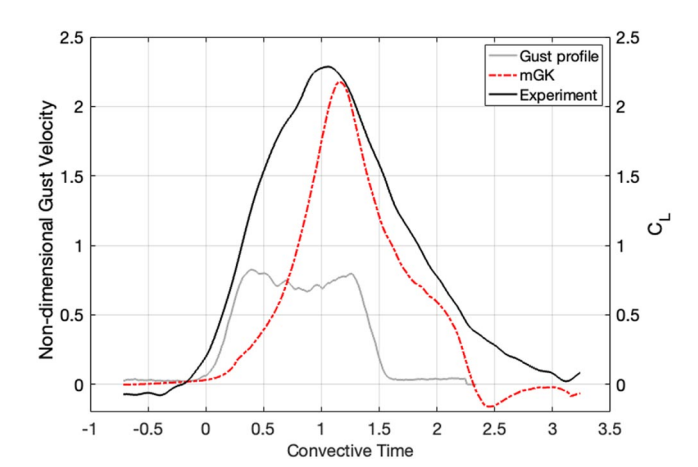


Fig. 4 Trapezoidal gust velocity profile (gray), lift coefficient of a non-maneuvering wing in the gust encounter measured in experiment (black), and lift coefficient predicted by the mGK model (red).

not explicitly part of the mGK model. The observation of a delay in the mGK response motivates the need to improve or augment the model so that it may be used to calculate optimal trajectories in real gust encounters. The IMO method in Sec. IV overcomes the delay in the mGK model and generates an optimized maneuver in a real experiment.

III. Optimal Control in a Transverse Gust Encounter Model

This section seeks an optimal, open-loop maneuver to regulate lift in a transverse gust encounter about a constant value, and presents an existing framework for optimal control design during a fixed-time interval with terminal constraints. It then applies this framework for a gust encounter represented by an mGK model.

A. Optimal Trajectory Problem with Terminal States Partially Specified

Consider a fixed-time interval $[t_0, t_f]$ during which an optimal control is sought, and let $x_j(t_f) = x_{f,j}$ for $j = 1, \ldots, p$ be state components specified at the terminal time. Note that p < n indicates partial specification of the terminal state, and it is assumed that all specified states appear before unspecified states in the state vector. The optimal-trajectory problem seeks an open-loop optimal control signal u that solves

min
$$J(u) = \int_{t_0}^{t_f} L(\mathbf{x}, u, t) dt$$

subject to $\dot{\mathbf{x}} = f(\mathbf{x}, u, t)$ with $\mathbf{x}(t_0) = \mathbf{x_0}$ (15)
 $0 = \psi(\mathbf{x}(t_f))$

where $L(\cdot)$ is the integrand of the performance measure J, $f(\cdot)$ represents the system dynamics, and $\psi(\cdot)$ is a vector of terminal constraints for p specified states, such that $\psi_j = x_j(t_f) - x_{f,j}$ for $j = 1, \ldots, p$. Equation (15) represents an optimal-control problem subject to the systems dynamics as a constraint and some state variables constrained at the terminal time.

The performance measure J in the optimal control problem (15) can be rewritten by adjoining the terminal state constraints using a Lagrange multiplier vector ν and adjoining the system dynamics using a vector of time-varying Lagrange multipliers known as costates λ . The augmented performance measure is

$$\tilde{J} = \boldsymbol{\nu}^T \boldsymbol{\psi}(\boldsymbol{x}(t_f)) + \int_{t_0}^{t_f} L(\boldsymbol{x}, u, t) + \boldsymbol{\lambda}^T (\boldsymbol{f} - \dot{\boldsymbol{x}}) \, \mathrm{d}t$$
 (16)

Note that if the terminal and dynamic constraints are satisfied, \tilde{J} equals J. To derive the first-order necessary conditions for stationarity, it is useful to define a Hamiltonian function $H = L + \lambda^T f$. Using techniques from the calculus of variations, the first-order necessary conditions for stationarity are [49]

$$\dot{\mathbf{x}} = \left(\frac{\partial H}{\partial \lambda}\right)^T$$
, with $\mathbf{x}(t_0) = \mathbf{x}_0$ (17)

$$\dot{\lambda} = -\left(\frac{\partial H}{\partial \mathbf{x}}\right)^T, \quad \text{with } \lambda_j(t_f) = \begin{cases} \nu_j, & j = 1, \dots, p \\ 0, & j = p + 1, \dots, n \end{cases}$$
 (18)

$$0 = \frac{\partial H}{\partial u} \tag{19}$$

$$x_i(t_f) = x_{f,i}, \quad \text{for } j = 1, \dots, p$$
 (20)

An optimal control u must satisfy conditions (17–20), which form a two-point boundary-value problem, with initial states and some terminal states specified.

Bryson and Ho [49] present a gradient-based method to solve for a candidate optimal control signal that satisfies Eqs. (17-20). For an initial guess of control signal u_0 , the corresponding state trajectory x can be determined from Eq. (17). The costate values at the terminal time should satisfy Eq. (18); however, the Lagrange multiplier vector ν is not known a priori. The method of Bryson and Ho [49] solves the costate Eq. (18) from a zero terminal condition $\lambda(t_f) = \mathbf{0}$ backward in time, which corresponds to a costate solve in a problem without state components specified at the terminal time. To deal with state constraints at the terminal time, Bryson and Ho [49] solve the co-state equation (18) several more times from altered terminal conditions in which the jth entry of λ is 1 and all other entries are 0 for j = 1, ..., p. These integrations are known as influence or sensitivity solves, because they provide costate trajectories that are useful in determining how the jth component of $x(t_f)$ is affected by a change in the control signal. Collecting the terminal conditions together in the columns of an influence matrix R at time t_f , the influence costate trajectories can be determined simultaneously by solving the matrix differential equation [49]

$$\dot{\mathbf{R}} = -\left(\frac{\partial \mathbf{f}}{\partial \mathbf{x}}\right)^T \mathbf{R}, \qquad \mathbf{R}_{ij}(t_f) = \begin{cases} 1, i = j, & i = 1, \dots, n \\ 0, i \neq j, & j = 1, \dots, p \end{cases}$$
(21)

using the solution of Eq. (21), Bryson and Ho [49] define integrals useful in calculating the Lagrange multiplier vector ν , which appears in the terminal condition of Eq. (18). They subsequently update the control guess in the $-\partial H/\partial u$ direction. Algorithm 1 presents the numerical method of Bryson and Ho [49], which is designed to iteratively improve the control signal, moving it closer to satisfying the necessary conditions and boundary conditions in Eqs. (17–20) with each step.

Previous work of the authors [34] showed that Algorithm 1 worked well for ideal, sine-squared gusts with various strengths and widths. Here, the mGK model and Algorithm 1 are applied to

Algorithm 1: Optimal control algorithm for fixed-time problems with partially specified terminal state [49]

Input: Initial guess of control signal u_0 .

- 1) Solve the state equation numerically from $x(t_0)$ to t_f .
- 2) Using the state trajectory obtained in step 1, numerically solve the costate Eq. (18) backward from $\lambda(t_f)=0$, and the influence performance in Eq. (21).
- 3) Calculate the following integrals:

$$I_{\psi\psi} = \int_{t_0}^{t_f} \mathbf{R}^T \frac{\partial \mathbf{f}}{\partial u} \Xi^{-1} \frac{\partial \mathbf{f}^T}{\partial u} \mathbf{R} \, \mathrm{d}t$$

$$I_{J\psi} = I_{\psi J}^T = \int_{t_0}^{t_f} \left(\lambda^T \frac{\partial \mathbf{f}}{\partial u} + \frac{\partial L}{\partial u} \right) \Xi^{-1} \frac{\partial \mathbf{f}^T}{\partial u} \mathbf{R} \, \mathrm{d}t$$

$$I_{JJ} = \int_{t_0}^{t_f} \left(\lambda^T \frac{\partial \mathbf{f}}{\partial u} + \frac{\partial L}{\partial u} \right) \Xi^{-1} \left(\lambda^T \frac{\partial \mathbf{f}}{\partial u} + \frac{\partial L}{\partial u} \right)^T \, \mathrm{d}t \quad (22)$$

where the weight matrix Ξ is a user-defined, positive-definite matrix that influences the step size of the algorithm.

- 4) Evaluate the stopping criteria to determine if the current control signal is satisfactory. Stop when $\psi(x(t_f)) = 0$ and $I_{JJ} I_{J\psi}I_{\psi\psi}^{-1}I_{\psi J} = 0$, to within desired tolerance.
- 5) Select a value of ϵ for a desired update in the terminal constraint, $\delta \psi = -\epsilon \psi(x(t_f))$, $0 < \epsilon \le 1$, to obtain the Lagrange-multiplier vector

$$\nu = -I_{ww}^{-1}(\delta \psi + I_{wJ}) \tag{23}$$

Update the control signal u according to

$$\delta u(t) = -\Xi^{-1} \left(\frac{\partial L}{\partial u} + (\lambda(t) + \mathbf{R}\nu)^T \frac{\partial L}{\partial u} \right)^T$$
 (24)

and return to step 1.

Output: Optimal control signal u.

calculate an optimal pitch maneuver when encountering the time-averaged velocity profile of a trapezoidal gust, based on the experimental gust profile from Fig. 4. Since the gust profile does not change during the wing–gust encounter, the gust is assumed to be nondeforming. For certain gusts, gust deformation does not strongly influence the lift force during the encounter, as examined in DVM calculations in [7].

B. Optimal Control Problem Using the mGK Model

Before the gust encounter, the wing flies at a steady reference flight condition

$$\begin{bmatrix} x_1(t_0) \\ x_2(t_0) \\ x_3(t_0) \end{bmatrix} = \begin{bmatrix} \theta_{g,ref} \\ \dot{\theta}_{g,ref} \\ q_{ref} \end{bmatrix}$$
 (25)

that corresponds to a constant lift coefficient $C_{L,\mathrm{ref}}$ for $\dot{\theta}_{g,\mathrm{ref}} = 0$. Lift regulation seeks to maintain the lift coefficient as close as possible to the reference value $C_{L,\mathrm{ref}}$. To implement C_L regulation, this paper uses pitch acceleration $\ddot{\theta}_g$ as the control input, such that $u = \ddot{\theta}_g$.

An appropriate performance measure for penalizing deviations of the output lift coefficient from the reference lift coefficient is

$$J = \frac{1}{2} \int_{t_0}^{t_f} (y - C_{L,\text{ref}})^2 dt$$
 (26)

Therefore, the integrand of the performance measure of Eq. (15) becomes

$$L(\mathbf{x}, u, t) = \frac{1}{2} \left(C_1(\alpha_{\text{eff}} - C_3) x_3 + C_2(\alpha_{\text{eff}} - C_4) (1 - x_3) + C_5 \overline{V} \left(x_2 - \frac{ab}{\overline{V}} u \right) - C_{\text{L,ref}} \right)^2$$
(27)

The terminal time t_f is chosen to be 14 time constants τ_1 after the time that the trailing edge leaves the gust. This choice is based on the time required for the lift signal observed in the nonmaneuvering experiment in Fig. 4 to return near zero. At the terminal time, the wing's state should return to the same reference flight condition that it had before the gust encounter, as shown in Eq. (25). However, constraining all states at the terminal time greatly reduces the performance of Algorithm 1 for a lift regulation problem, because the algorithm tries to pitch the wing to strictly enforce $q(t_f) = q_{ref}$ at the terminal time. The dynamics of the mGK model naturally drive q to $q_{\rm ref}$ after the wing stops maneuvering. Hence, strictly enforcing $q(t_f) = q_{ref}$ is not necessary in practice. Requiring that $\theta_g(t_f) = \theta_{g,ref}$ and $\dot{\theta}_g(t_f) = \dot{\theta}_{g,ref}$ at the terminal time and penalizing deviations of the output from $C_{L,ref}$ are sufficient to ensure that $q(t_f)$ is nearly equal to q_{ref} for the terminal time t_f selected in this work. By constraining only two of the three state components at the terminal time, the terminalconstraint vector becomes

$$\psi(\mathbf{x}(t_f)) = \begin{bmatrix} x_1(t_f) - \theta_{g,ref} \\ x_2(t_f) - \dot{\theta}_{g,ref} \end{bmatrix}$$
 (28)

The mGK model and the selection of the performance measure, time interval, and initial and terminal conditions fully specify the optimal-trajectory problem for lift regulation. Remaining details of derivatives necessary to implement Algorithm 1 are available in [34].

The optimal-control framework was applied in simulation to a wing at a reference angle of attack of 0 deg, surging through the trapezoidal gust with gust ratio GR = 0.7 at a constant speed of 0.118 m/s (Re = 12,000). The reference flight conditions are therefore $C_{L,\mathrm{ref}} = 0$, $\dot{\theta}_{g,\mathrm{ref}} = 0$, and $q_{\mathrm{ref}} = 1$. Figure 5a presents the simulated lift coefficients for a nonmaneuvering wing (blue line) and a wing pitching according to the open-loop, optimal-control calculation (black line). In Fig. 5b, note that the optimal control input $\ddot{\theta}_g$ is nearly zero after convective time $t^* = 4$, which shows that this solution is not sensitive to a small change in the terminal time t_f .

C. Comparison to Proportional Output-Feedback Control

Sedky et al. [7] used proportional output-feedback of the lift signal to pitch a flat plate in a transverse gust encounter modeled using a DVM. In [7], the proportional output-feedback

controller effectively regulated lift, which motivates a comparison of proportional output-feedback control to the optimal control results derived in this paper. The proportional output-feedback controller is

$$u_{\text{out}} = -K(C_L - C_{L,\text{ref}})$$

$$= -K \left(C_1(\alpha_{\text{eff}} - C_3)q + C_2(\alpha_{\text{eff}} - C_4)(1 - q) + C_5 \left(\dot{\theta}_g - \frac{ab}{\overline{V}} \ddot{\theta}_g \right) - C_{L,\text{ref}} \right)$$
(29)

where K is a constant feedback gain that must be selected. This section tests a sequence of different K values for the trapezoidal gust profile.

Figure 6a shows simulation results for a wing encountering a gust while applying proportional output-feedback control for several choices of feedback gain K. When the gain is small, the lift regulation is poor, but the performance significantly improves as K increases. Figure 6b shows the corresponding control signals. Note that proportional output-feedback control signal closely aligns with the optimal control signal for $K \ge 100$. The simulation results indicate that the proportional output-feedback controller is optimal for a sufficiently large K. This numerical observation suggests that open-loop optimal control signals can be generated for the mGK model of this paper without optimal control calculations; only simulation of the mGK model with the control choice in Eq. (29) is needed. This finding is useful because the computational cost for a proportional output-feedback simulation is much lower than the cost of an optimal trajectory calculation. Thus, one can rapidly generate the optimal pitch maneuver in the IMO method presented in the next section. However, it is important to note that the consideration of proportional output-feedback control as optimal for very large gains, as suggested numerically here, should be limited to the generation of open-loop trajectories in simulation. Real experimental data contain noise that could be amplified by the feedback gain of a high-gain controller, which would lead to poor lift regulation in practice.

IV. Iterative Construction of an Optimal Maneuver

The optimal-control algorithm of Sec. III provides an optimal-control signal based on the mGK model for the wing-gust encounter. However, as noted in Sec. II.D, there is a delay in the lift response of the mGK model in comparison to experimental

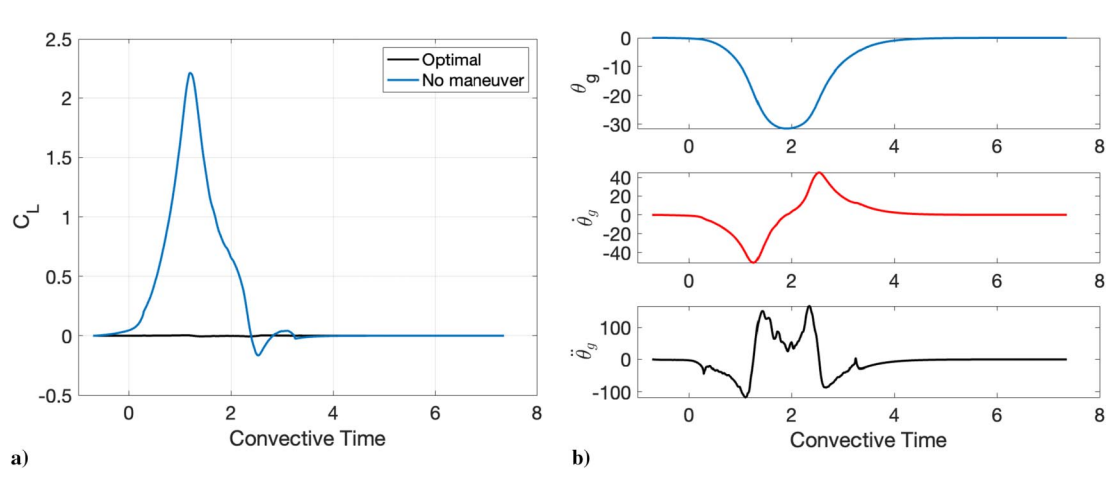


Fig. 5 Simulation results for encounters with a trapezoidal gust using the mGK model. a) Lift coefficients for nonmaneuvering and optimally maneuvering wings. b) Control profiles of the optimal maneuver.

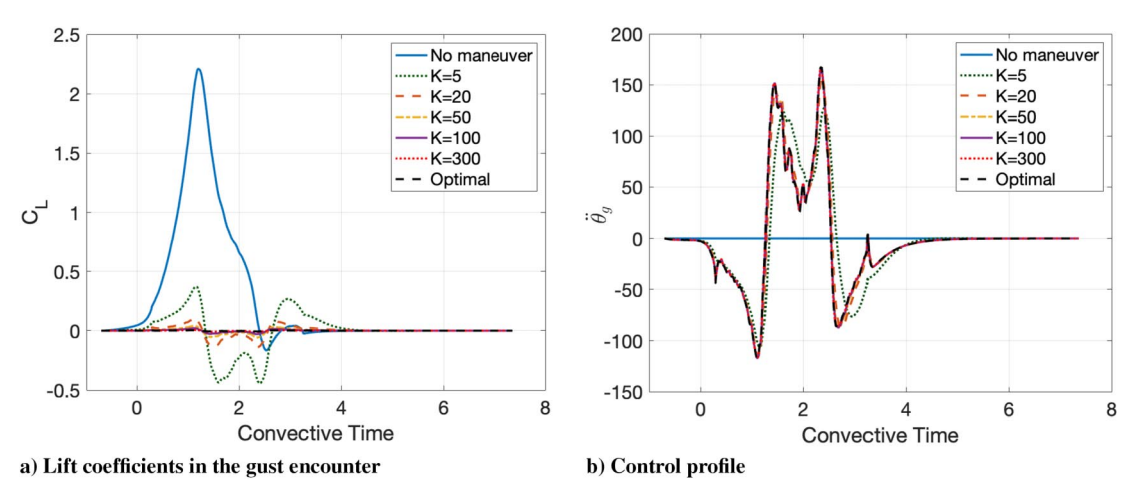


Fig. 6 Simulation results for a) lift coefficient and b) pitch acceleration input for encounters with a trapezoidal gust using proportional output-feedback control.

measurements. It is important to develop a method that can generate optimal-control signals for real-gust flows. This section employs the useful, yet imperfect, mGK model to develop an iterative-optimization method applicable to real-gust flows.

A. Iterative Maneuver Optimization

Figure 4 shows the result of unmodeled vortex shedding in the mGK model, whereby the experimental lift measurements rise faster than the predicted lift as the wing enters the gust between convective times 0 and 1. One possible solution to this model-error problem is to pitch the wing in anticipation of the delayed response of the model. One approach to implement such a model correction is to update the reference signal for tracking. In a regulation problem, the reference signal is a constant. However, altering the reference signal can feed-forward information about model deficiencies. The IMO method that this paper proposes takes into account force errors due to unmodeled effects and updates the control profile accordingly. To illustrate the proposed procedure, assume that an open-loop optimal-pitch maneuver derived by the optimal-control framework presented in Sec. III.B predicts a lift coefficient that is labeled as $C_{L,\mathrm{model}}^{(1)}$. In general, the lift coefficient predicted by the mGK model on the *i*th iteration is $C_{L,\text{model}}^{(i)}$, and the derived optimal-pitch maneuver can be tested in experiment or in a higher fidelity simulation to provide the measured lift coefficient $C_{L,\mathrm{test}}^{(i)}$. Note that the lift coefficient predicted by the mGK model in the first iteration, $C_{L,\text{model}}^{(1)}$, is nearly the reference $C_{L,\text{ref}}$. Ideally, the $C_{L,\text{test}}^{(i)}$ would be close to $C_{L,\text{model}}^{(i)}$, but there are some unmodeled effects, and thus the error between the measured and modeled lift coefficients in the i th iteration is

$$\Delta C_L^{(i)} = C_{L,\text{test}}^{(i)} - C_{L,\text{model}}^{(i)} \tag{30}$$

The cost function in Eq. (26) seeks to find a $C_{L,\text{model}}$ that minimizes the deviation of the lift coefficient from a reference lift coefficient signal during a simulated gust encounter. The errors from Eq. (30) can update the reference lift coefficient according to

$$C_{L,\text{ref}}^{(i+1)} = C_{L,\text{ref}} - \Delta C_L^{(i)}$$
 (31)

Note that Eqs. (30) and (31) are equations of C_L signals over the time interval $[t_0, t_f]$.

With the new reference lift curve, one can derive a new optimalcontrol signal to minimize the modified performance measure

$$\hat{J} = \frac{1}{2} \int_{t_{-}}^{t_{f}} \left(C_{L,\text{model}}^{(i+1)}(t) - C_{L,\text{ref}}^{(i+1)}(t) \right)^{2} dt$$
 (32)

which penalizes the differences between the model prediction $C_{L,\mathrm{model}}^{(i+1)}$ and the new reference lift coefficient $C_{L,\mathrm{ref}}^{(i+1)}$. The new optimal-control profile can be applied in experiment again, and repeating this procedure several times causes the $C_{L,\mathrm{test}}$ signal to approach the ideal reference lift $C_{L,ref}$. Algorithm 2 summarizes this procedure, which the authors refer to as iterative maneuver optimization (IMO). As an example of these equations, at a particular time t_p , consider the case in which $C_{L,\mathrm{test}}(t_p)$ is greater than $C_{L,\mathrm{model}}(t_p)$. Then, the error $\Delta C_L(t_p)$ indicates that the new reference lift coefficient $C_{L,\mathrm{ref}}^{(i+1)}$ should be reduced according to Eq. (31). The optimalcontrol framework would then generate a control signal such that $C_{L,\text{model}}(t_p)$ closely matches $C_{L,\text{ref}}^{(i+1)}(t_p)$. The new control signal seeks to produce less lift in anticipation of encountering the excess in lift that occurred during the previous test, thereby compensating for an unmodeled effect. As discussed in Sec. III.C, the optimalcontrol framework requires nonnegligible computation time, but high-gain, proportional output-feedback control can rapidly generate the optimal-control profile for the mGK model. Exploiting the correspondence between the optimal-control and the high-gain feedback results can lead to significant time savings for the IMO method. The updated control signal derives from the outputfeedback control law

$$u_{\text{out}}^{(i+1)} = -K(C_{L,\text{model}}^{(i+1)} - C_{L,\text{ref}}^{(i)})$$
(33)

Note that due to the appearance of (i + 1) at both sides of Eq. (33), the control signal must be generated during the closed-loop simulation of the mGK model.

The IMO method only requires the mGK model and several runs through the experiment or higher-fidelity model to generate an optimal maneuver for the higher-fidelity system. Notably, it does not require any real-time feedback signals within the higher-fidelity system to update the control profile. Although the surrogate model (i.e., the mGK model) is not very accurate, it is computationally cheap to optimize using output-feedback control. Iterative implementation and refinement of the maneuver helps to overcome the inaccuracies of the surrogate model.

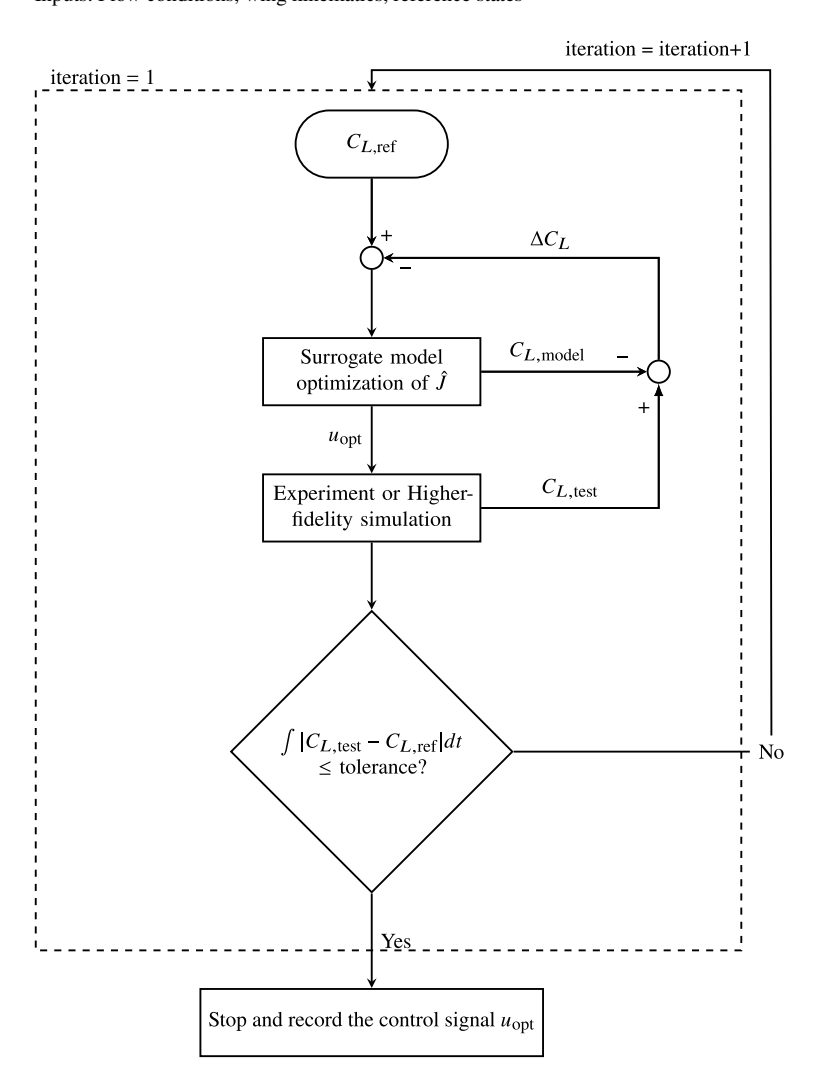
B. Numerical Implementation of Iterative Maneuver Optimization

The IMO method is first implemented numerically using a DVM in place of physical experiments. The DVM represents a higher-fidelity model, because it captures vortex shedding that is not explicitly part of the mGK model. Note that one could alternately use computational fluid dynamics (CFD) simulations for the high-fidelity model, but the time per iteration would greatly increase.

The DVM in this work has LEV shedding that is either turned on or off according to the value of the leading-edge suction parameter (LESP). Hence, the simulation is called an LESP-modulated DVM

Algorithm 2: Iterative maneuver optimization method

Inputs: Flow conditions, wing kinematics, reference states



Output: Optimal pitch maneuver $\ddot{\theta}_{\varrho} = u_{\text{opt}}$

(LDVM). A prescribed velocity field represents the gust, and the wing sheds vorticity in response to the flowfield and kinematic maneuvering. The LESP is a nondimensional quantity introduced by Ramesh et al. [24] that serves as the criterion of leading-edge shedding. When the LESP value exceeds the critical value LESPc, which is determined empirically from experimental or CFD data, the airfoil sheds vortices from the leading edge. Otherwise, only the trailing edge of the airfoil sheds vortices according to a Kelvin condition [50]. For additional information regarding the construction of the LDVM used in this work and the lift force calculation from the LDVM model, please refer to [26].

A common issue for DVMs is overprediction of lift due to their omission of viscous effects [51]. To address this issue, this paper compares the experimental, steady-lift curve slope for attached flow that is used in the mGK model to the ideal 2π slope from thin-airfoil theory. To better predict the lift coefficient, the LDVM lift coefficient is multiplied by $C_1/2\pi$ to provide closer agreement with experimental measurements. Figure 7 presents the lift coefficient results for a nonmaneuvering wing encountering a trapezoidal gust with a gust ratio GR = 0.7. The blue dashed line is the LDVM simulation result, which includes the empirical $C_1/2\pi$ lift adjustment. The black line is

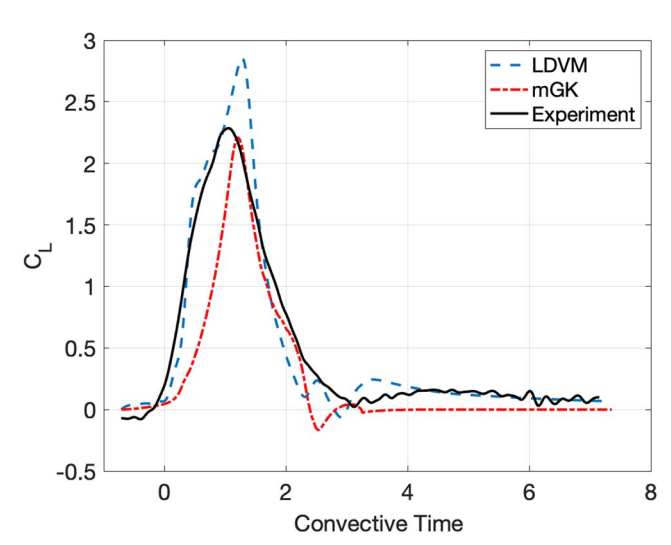


Fig. 7 Simulations of a nonmaneuvering wing during the gust encounter of a trapezoidal gust.

the experimental measurement, and the red line is the simulation from the mGK model. The LDVM result matches the experimental data well during gust entry and exit, but it still overpredicts the lift peak. Note that the LDVM result more closely agrees with the experiment than the mGK model. Here, the LDVM represents a higher-fidelity model than the mGK model and can be used to test the IMO method before carrying out experimental validation.

The IMO method was performed with the LDVM simulation taking the place of the experiment in Algorithm 2 to produce $C_{L.\mathrm{test}}$. The surrogate model optimization in Algorithm 2 was highgain output-feedback control of the mGK model, which produced $C_{L.\mathrm{model}}$. The time-averaged velocity profile of the trapezoidal gust in Fig. 4 provided the external disturbance. For the LDVM simulation, the LESPc value was set to 0.18, which is a common value found in literature [24,52]. The LESPc value differs in a subsequent investigation of this section.

Figure 8 shows the results of the IMO method applied to the LDVM of the wing–gust encounter. The first iteration directly applied the optimal-control profile derived for the mGK model in the LDVM. Figure 8a shows a noticeable delay in lift response due to the known delay in the mGK model. However, the second iteration adjusted the $C_{L,\mathrm{ref}}$ signal and derived an optimal-control profile for tracking $C_{L,\mathrm{ref}}^{(2)}$. As a result, the regulation performance significantly improved. The performance of the maneuver improved further in the third iteration. Figure 8c shows the rapid convergence of lift to $C_{L,\mathrm{ref}}=0$ after five iterations. Figure 8e shows that the lift remained 0 for additional iterations. The simulation results show that the IMO method can successfully construct an optimal-pitching maneuver in only a few iterations.

The optimal pitch maneuver is shown in Fig. 8b. Figures 8d and 8f contain the pitch rate and the pitch acceleration, respectively. The

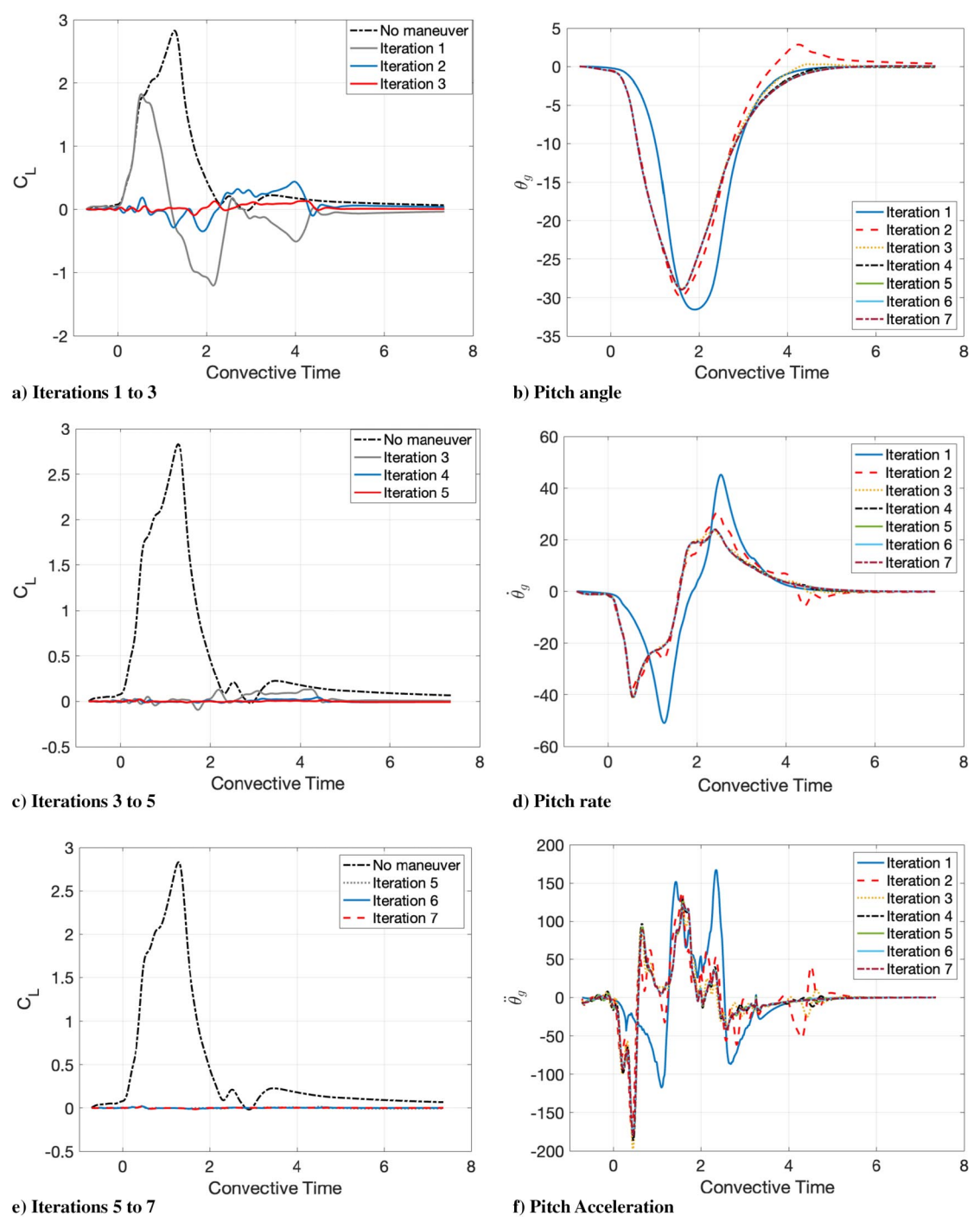


Fig. 8 IMO of a wing-gust encounter in an LDVM simulation.

wing generally pitched down, then up, to negate the lift overshoot in the gust encounter. In this simulation, the IMO method was able to eliminate lift deviations; however, the LDVM simulation is an ideal case since the flowfield is highly repeatable. The errors in the previous iteration can therefore be completely corrected in the next iteration until there are no errors between the desired output and the real output. In a real experiment, the flowfield may contain spurious disturbances that reduce run-to-run repeatability. Additionally, there may be many more effects not captured by the surrogate model. The Sec. V explores implementation of IMO in a real flowfield.

Figure 9 shows different moments during the gust encounter when the optimal-pitch maneuver derived in the mGK model was applied to the LDVM simulations. Each iteration shows vorticity in the flow-field during a pitch-down, then pitch-up maneuver. After the first iteration, changes in the wake of the wing at $t^* = 0.3$ indicate that IMO adjusted the maneuver to pitch down sooner during entry. At time $t^* = 1.2$, a large LEV is present that sheds over the upper surface of the wing. For subsequent IMO iterations, the size of the LEV is reduced and the location is further aft on the upper surface. Since this LEV during gust entry is associated with lift overshoot, the maneuver regulates lift by reducing its size and encouraging its shedding during

pitching. At time $t^* = 2.3$, both the first and second iterations show remnants of a high-pressure side LEV beneath the wing that is eliminated in subsequent iterations. Iteration 1 also shows the roll-up of a TEV with negative circulation (red) that does not roll up in subsequent iterations. In general, the optimal maneuver generated by IMO created fewer and smaller vortical structures during the encounter.

To further investigate the design of an optimal pitch maneuver in LDVM simulation using IMO, the LESPc value was reduced to 0.12, which corresponds with a greater tendency to shed from the leading edge. Figure 10 shows the lift coefficient of the wing during the gust encounters with LESPc = 0.12 for nine iterations of IMO. Although the lift coefficient in iteration 4 is small, the performance in subsequent iterations does not converge. In fact, lift deviations worsen and seem to oscillate between iterations. The IMO method cannot generate an ideal lift coefficient curve that is as flat as the LESPc = 0.18 case. Iteration-to-iteration oscillation of the lift curve continued in the IMO process after iteration 9. Nonetheless, the IMO method was able to significantly reduce lift deviations. The finding of oscillations indicates that the optimization process may not be able to further improve performance, and may need a stopping criterion that identifies a lack of further progress. Monitoring for an increase in the

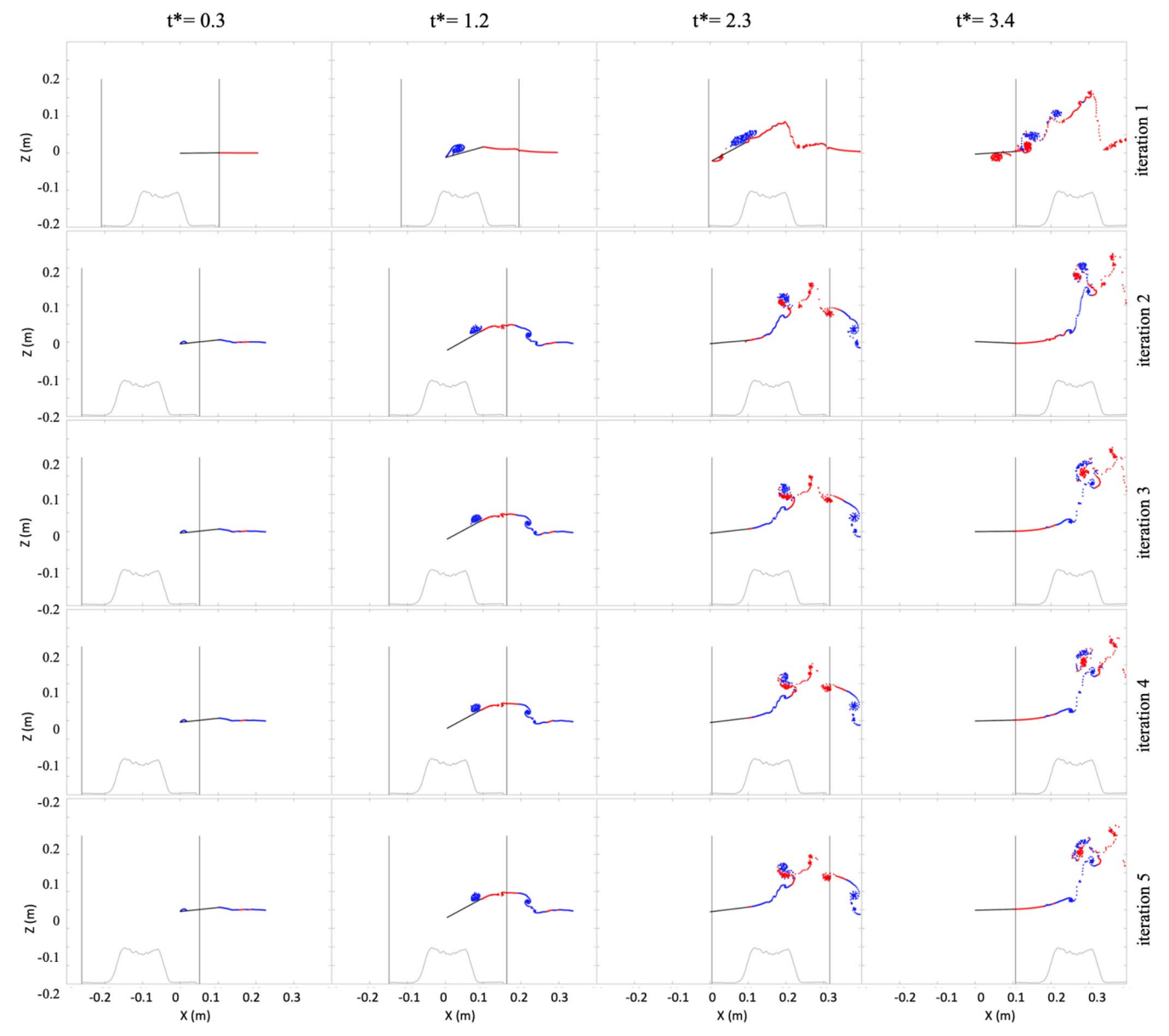


Fig. 9 Flow vorticity fields of the LDVM simulation for five IMO iterations with LESPc = 0.18.

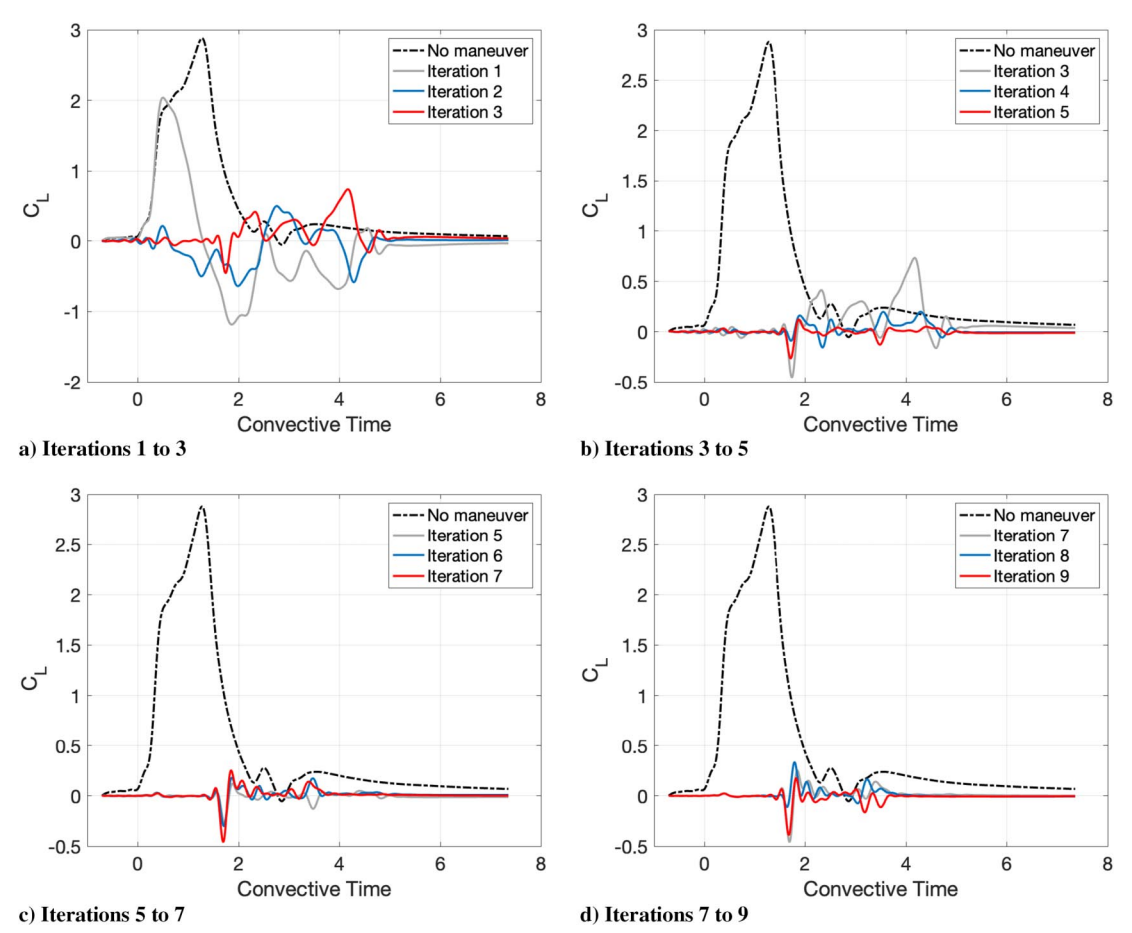


Fig. 10 LDVM Simulation results of the IMO method, LESPc = 0.12.

cost function J, for example, would have stopped to select the control signal at iteration 4 for the optimized maneuver.

Figure 11 presents the vorticity field of the LDVM simulations with LESPc = 0.12. Time $t^* = 0.3$ closely resembles the simulation in Fig. 9 with the higher LESPc value. However, at time $t^* = 1.2$, the LEV above the wing is larger in comparison to Fig. 9 for all iterations. After pitching down, LEVs with negative circulation strength (red) were shed on the high-pressure side of the wing, which can be observed at $t^* = 2.3$ in every iteration. Since the wing more easily shed LEVs than the higher LESPc case, the IMO method did not eliminate the high-pressure side LEVs at $t^* = 2.3$. Additionally, the wake behind the wing at $t^* = 2.3$ shows more iteration-to-iteration variation for the LESPc = 0.12 case than the LESPc = 0.18 case. The larger LEV that appears at $t^* = 1.2$ for LESPc = 0.12 may have caused greater wake variation when interacting with trailing-edge shed vorticity. The wing has very little control over vorticity in the wake, which may explain the inability of the IMO method to completely eliminate lift deviations for the LESPc = 0.12 case. Nonetheless, the control signal from iteration 4 did provide significant gust rejection for the maneuver determined by the IMO method.

V. Experimental Construction of an Optimal Pitch Maneuver

This section presents experimental validation of the IMO method in a water towing tank with a transverse gust generator. The experiments followed the same IMO procedure as the LDVM simulations, with the physical system replacing the LDVM. As described in Sec. IV, the first iteration applied the open-loop control profile derived by simulation of the mGK output-feedback control. The pitching mechanism actuated the wing, and the lift response was recorded. The measured output lift was used to update the desired reference lift signal for the wing to track. Performing an mGK output-

feedback control simulation provided a new optimal-control profile to test in experiment on the next iteration. Although the LDVM of the previous section provides a perfectly repeatable flowfield and lift signal for a given maneuver, the experiments contain experimental variation and sensor noise. Since noise may influence the control profile calculation, during each iteration, the control profile was run five times in the tow tank and the output lift coefficient was ensemble averaged. To examine continued iteration of the IMO method, a stopping criterion was not set. However, the experiment was terminated after iteration 7 due to the appearance of iteration-to-iteration oscillation in the lift deviations.

Figure 12 presents the experiment results of the IMO method applied to a NACA 0012 wing encountering the trapezoidal gust with gust ratio GR = 0.7. Figure 12a shows the first three iterations. The first iteration again exhibited a delay due to the surrogate model. The second iteration improved the lift regulation significantly, and the third iteration showed an even better result. These data show that the IMO method can improve open-loop control maneuvers in experiment. Figure 12c contains the results of iterations 3–5, where iteration 3 is retained from Fig. 12a for comparison. Iterations 4 and 5 show an improvement in the lift coefficient during the gust encounter in comparison to iteration 3, although some oscillations are present after the gust, between convective times $t^* = 5$ and $t^* = 7$. In iteration 5, the maximum absolute value of the lift coefficient is below 0.2 during the encounter time. This value is less than 8% of the peak value for the nonmaneuvering experiment, representing a 92% reduction in the lift overshoot. With continued iterations, Fig. 12e shows that the lift coefficient no longer improved, and in fact worsened in performance. Iterations 6 and 7 increased the amplitude of oscillation in the lift deviations. Continuation of the algorithm provided lift curves that oscillated between the convective times $t^* = 5$ and $t^* = 7$ without further improvement.

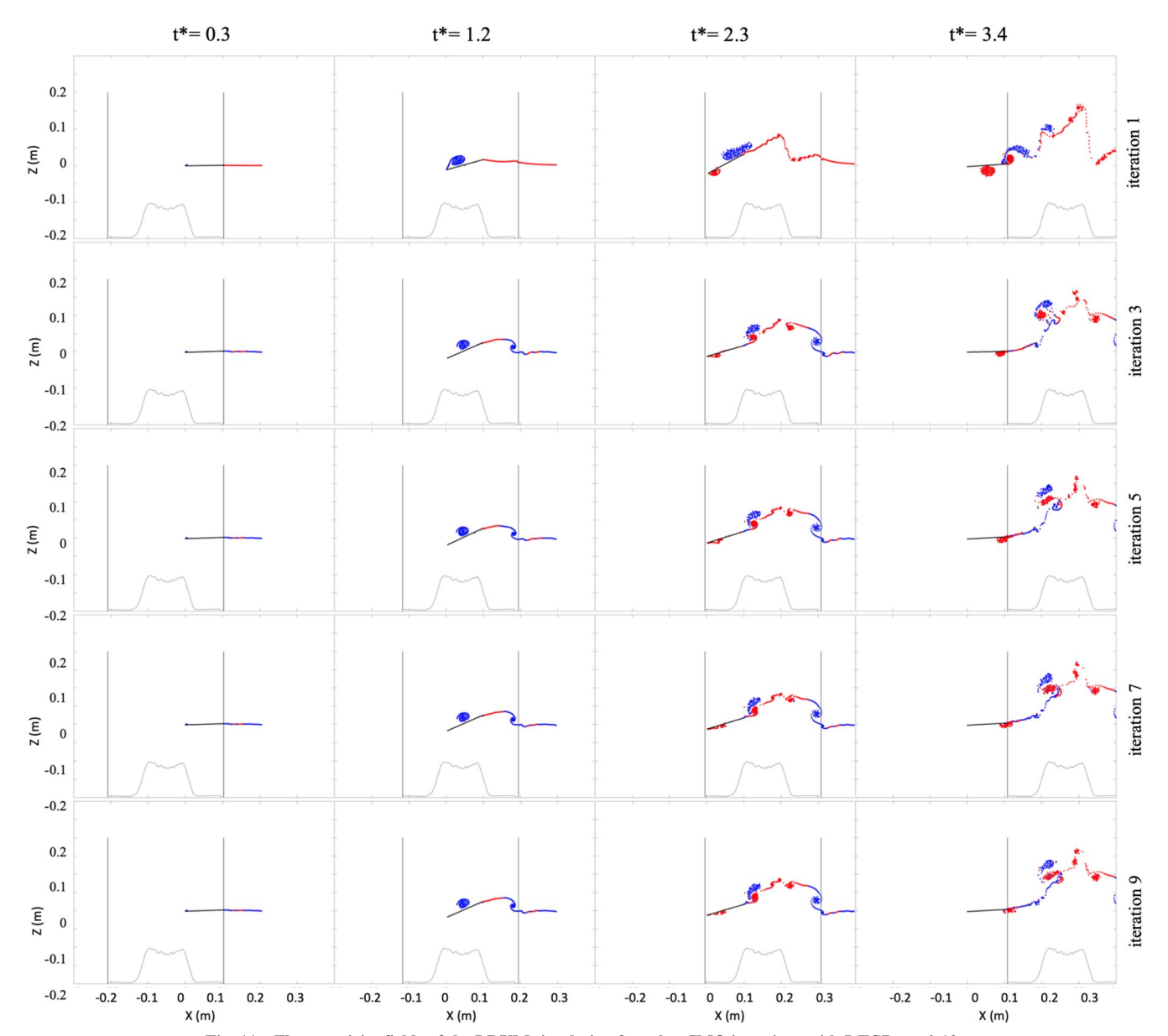


Fig. 11 Flow vorticity fields of the LDVM simulation for select IMO iterations with LESPc = 0.12.

The pitch maneuvers in Fig. 12b are pitch-down, then pitch-up maneuvers for all the iterations. The later iterations overcame the delay present in the first iteration. Since lift response did not improve after iteration 4, Figs. 12b, 12d, and 12f only include data from iterations 1 through 4 for clarity. The pitch angle profiles after iteration 2 agree during the gust encounter but deviate after the wing exits the gust. A possible explanation for the oscillations in the lift responses may be vibrations in the pitching mechanism, which were visible during the experiments. Unlike the aerodynamic lift, vibrations in the setup are not directly controllable by pitching the wing. Hence, the IMO method may have responded to vibrations in the output signals by giving unnecessary maneuver updates to the wing. In future work, experimental flowfield measurements, such as PIV, may yield further insight and provide a comparison to the LDVM simulations.

VI. Conclusions

This paper explores the generation of maneuvers that optimally regulate aerodynamic force on a wing when encountering an external flow disturbance. In particular, the paper studies a pitching wing in a transverse gust encounter. First, a gradient-based algorithm from optimal-control theory is applied to calculate an optimal-pitch

maneuver to regulate lift during a transverse gust encounter, subject to a modified GK model of the physics in the wing-gust encounter. The gradient-based method searches for a locally optimal solution. Simulation results indicate that a proportional output-feedback controller with a sufficiently large control gain can generate optimalcontrol solutions for an mGK model. However, comparison of the mGK model to experimental gust encounter data reveals a noticeable time delay due to unmodeled effects. To address unmodeled effects, this paper proposes an IMO method. The method generates a proposed maneuver by optimizing the tracking of a reference force signal in the mGK model. Then, testing in experiment or high-fidelity simulation is performed to update the reference signal according to deviations from the expected output force signal. A new candidate maneuver is generated by tracking the new reference signal, and the process repeats. Simulations show that the IMO method can overcome the time-delay problem of the surrogate mGK model to generate an optimal maneuver. Experimental results in a water towing tank demonstrated that the IMO method can construct an optimal pitch maneuver in a real gust encounter. Small oscillations in the lift coefficient remained in the experimental results, but an overall 92% reduction in the lift overshoot was obtained in experiment.

In future work, the authors are interested in collecting flowfield measurements, such as PIV during the iteration process. The authors

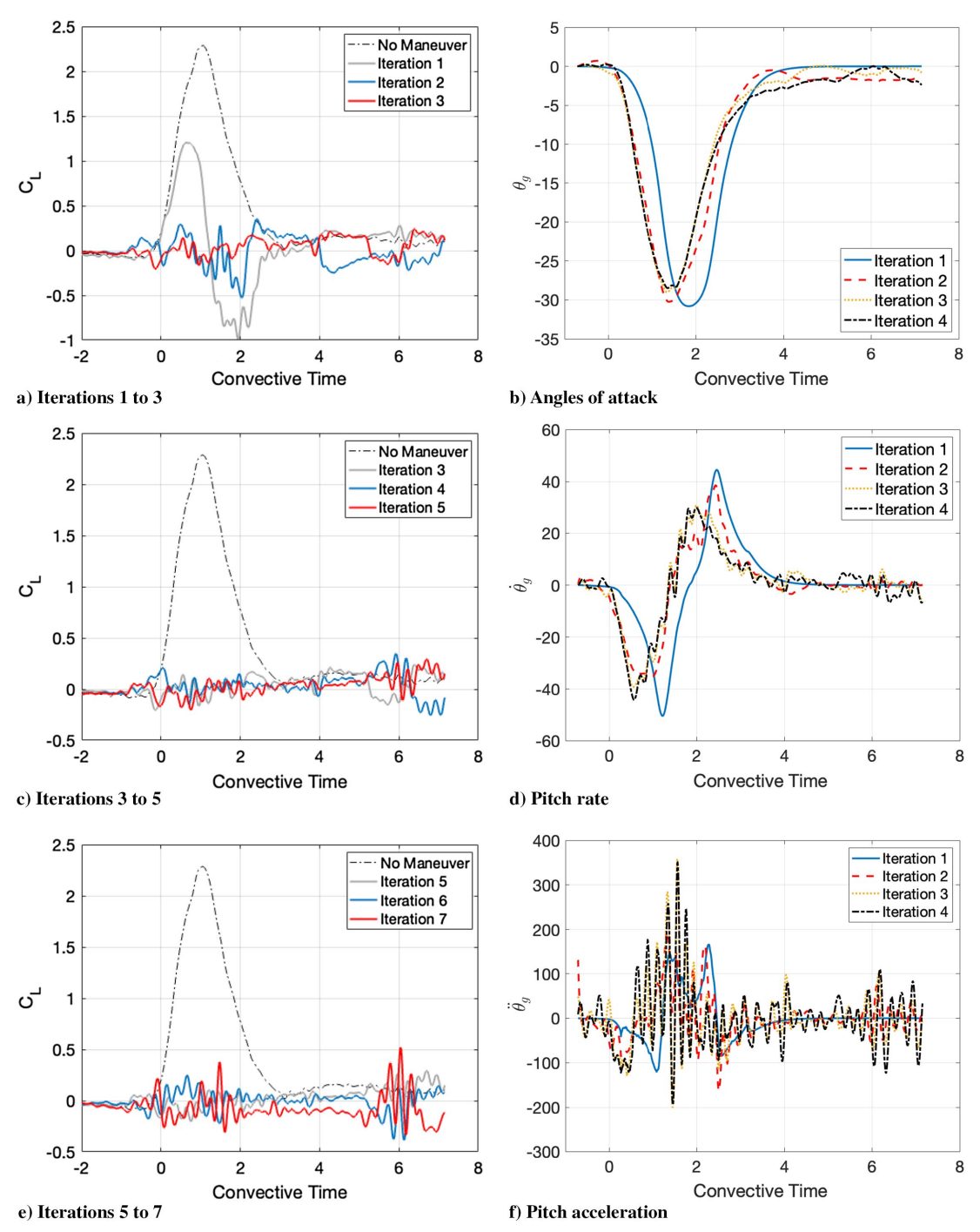


Fig. 12 Experimental results of the IMO method.

may also examine application of the IMO method to other types of gusts, wings, and methods of actuation.

Acknowledgments

This work was supported by the National Science Foundation under grant CBET-2003999, monitored by program officer R. Joslin. The authors gratefully acknowledge valuable discussions with J. Graff, A. SureshBabu, A. Gopalarathnam, and T. Singh. The authors thank the anonymous reviewers for suggestions that greatly improved this paper.

References

[1] Zarovy, S., Costello, M., Mehta, A., Gremillion, G., Miller, D., Ranganathan, B., Humbert, J. S., and Samuel, P., "Experimental Study of Gust Effects on Micro Air Vehicles," AIAA Atmospheric Flight Mechanics Conference, AIAA Paper 2010-7818, 2010.

- [2] Biler, H., Badrya, C., and Jones, A. R., "Experimental and Computational Investigation of Transverse Gust Encounters," *AIAA Journal*, Vol. 57, No. 11, 2019, pp. 4608–4622. https://doi.org/10.2514/1.J057646
- [3] Andreu-Angulo, I., Babinsky, H., Biler, H., Sedky, G., and Jones, A. R., "Effect of Transverse Gust Velocity Profiles," AIAA Journal, Vol. 58, No. 12, 2020, pp. 5123–5133. https://doi.org/10.2514/1.J059665
- [4] Sedky, G., Jones, A. R., and Lagor, F. D., "Lift Regulation During Transverse Gust Encounters Using a Modified Goman–Khrabrov Model," AIAA Journal, Vol. 58, No. 9, 2020, pp. 1–11. https://doi.org/10.2514/1.J059127
- [5] Andreu-Angulo, I., and Babinsky, H., "Unsteady Modelling of Pitching Wings for Gust Mitigation," AIAA Scitech 2021 Forum, AIAA Paper 2021-1999, 2021. https://doi.org/10.2514/6.2021-1999
- [6] Andreu-Angulo, I., and Babinsky, H., "Negating Gust Effects by Actively Pitching a Wing," AIAA Scitech 2020 Forum, AIAA Paper

- 2020-1057, 2020. https://doi.org/10.2514/6.2020-1057
- [7] Sedky, G., Lagor, F. D., and Jones, A. R., "Unsteady Aerodynamics of Lift Regulation During a Transverse Gust Encounter," *Physical Review Fluids*, Vol. 5, No. 7, 2020, Paper 074701. https://doi.org/10.1103/PhysRevFluids.5.074701
- [8] Moulin, B., and Karpel, M., "Gust Loads Alleviation Using Special Control Surfaces," *Journal of Aircraft*, Vol. 44, No. 1, 2007, pp. 17–25. https://doi.org/10.2514/1.19876
- [9] Cook, R. G., Palacios, R., and Goulart, P., "Robust Gust Alleviation and Stabilization of Very Flexible Aircraft," *AIAA Journal*, Vol. 51, No. 2, 2013, pp. 330–340. https://doi.org/10.2514/1.J051697
- [10] Bhatia, M., Patil, M., Woolsey, C., Stanford, B., and Beran, P., "Stabilization of Flapping-Wing Micro-Air Vehicles in Gust Environments," *Journal of Guidance, Control, and Dynamics*, Vol. 37, No. 2, 2014, pp. 592–607. https://doi.org/10.2514/1.59875
- [11] Oduyela, A., and Slegers, N., "Gust Mitigation of Micro Air Vehicles Using Passive Articulated Wings," *Scientific World Journal*, Vol. 2014, Jan. 2014, Paper 598523.
- [12] Moushegian, A., Weston, C., and Smith, M. J., "Analysis of a Wing Moving Through a Nonlinear Gust," AIAA Scitech 2019 Forum, AIAA Paper 2019-0637, Jan. 2019. https://doi.org/10.2514/6.2019-0637
- [13] Grubb, A. L., Moushegian, A., Heathcote, D. J., and Smith, M. J., "Physics and Computational Modeling of Nonlinear Transverse Gust Encounters," AIAA Scitech 2020 Forum, AIAA Paper 2020-0080, 2020.
- [14] Leishman, G. J., Principles of Helicopter Aerodynamics, Cambridge Univ. Press, Cambridge, England, U.K., 2006, Chap. 8.
- [15] Xu, X., and Lagor, F. D., "Quasi-Steady Effective Angle of Attack and Its Use in Lift-Equivalent Motion Design," *AIAA Journal*, Vol. 59, No. 7, 2021, pp. 2613–2626. https://doi.org/10.2514/1.J059663
- [16] Theodorsen, T., and Mutchler, W., "General Theory of Aerodynamic Instability and the Mechanism of Flutter," National Advisory Committee for Aeronautics NACA-TR-496, Washington, D.C., 1935.
- [17] Wagner, H., "Über die Entstehung des Dynamischen Auftriebes von Tragflügeln," ZAMM-Journal of Applied Mathematics and Mechanics/ Zeitschrift für Angewandte Mathematik und Mechanik, Vol. 5, No. 1, 1925, pp. 17–35. https://doi.org/10.1002/zamm.19250050103
- [18] Küssner, H. G., "Zusammenfassender Bericht über den Instationären Auftrieb von Flügeln," *Luftfahrtforschung*, Vol. 13, No. 12, 1936, pp. 410–424.
- [19] von Kármán, T., "Airfoil Theory for Non-Uniform Motion," *Journal of the Aeronautical Sciences*, Vol. 5, No. 10, 1938, pp. 379–390. https://doi.org/10.2514/8.674
- [20] Badrya, C., Biler, H., Jones, A. R., and Baeder, J. D., "Effect of Gust Width on Flat-Plate Response in Large Transverse Gust," *AIAA Journal*, Vol. 59, No. 1, 2021, pp. 49–64. https://doi.org/10.2514/1.J059678
- [21] Perrotta, G., and Jones, A. R., "Unsteady Forcing on a Flat-Plate Wing in Large Transverse Gusts," *Experiments in Fluids*, Vol. 58, No. 8, 2017, pp. 1–11. https://doi.org/10.1007/s00348-017-2385-z
- [22] Jones, A. R., Cetiner, O., and Smith, M. J., "Physics and Modeling of Large Flow Disturbances: Discrete Gust Encounters for Modern Air Vehicles," *Annual Review of Fluid Mechanics*, Vol. 54, Jan. 2022, pp. 469–493. https://doi.org/10.1146/annurev-fluid-031621-085520
- [23] Darakananda, D., da Silva, A. F. C., Colonius, T., and Eldredge, J. D., "Data-Assimilated Low-Order Vortex Modeling of Separated Flows," *Physical Review Fluids*, Vol. 3, No. 12, 2018, Paper 124701. https://doi.org/10.1103/PhysRevFluids.3.124701
- [24] Ramesh, K., Gopalarathnam, A., Granlund, K., Ol, M. V., and Edwards, J. R., "Discrete-Vortex Method with Novel Shedding Criterion for Unsteady Aerofoil Flows with Intermittent Leading-Edge Vortex Shedding," *Journal of Fluid Mechanics*, Vol. 751, July 2014, pp. 500–538. https://doi.org/10.1017/jfm.2014.297
- [25] Narsipur, S., Gopalarathnam, A., and Edwards, J. R., "Low-Order Model for Prediction of Trailing-Edge Separation in Unsteady Flow," *AIAA Journal*, Vol. 57, No. 1, 2019, pp. 191–207. https://doi.org/10.2514/1.J057132.
- [26] Sureshbabu, A. V., Medina, A., Rockwood, M., Bryant, M., and Gopalarathnam, A., "Theoretical and Experimental Investigation of an Unsteady Airfoil in the Presence of External Flow Disturbances," *Journal of Fluid Mechanics*, Vol. 921, Aug. 2021, p. A21. https://doi.org/10.1017/jfm.2021.484

- [27] Hou, W., Darakananda, D., and Eldredge, J. D., "Machine-Learning-Based Detection of Aerodynamic Disturbances Using Surface Pressure measurements," AIAA Journal, Vol. 57, No. 12, 2019, pp. 5079–5093. https://doi.org/10.2514/1.J058486
- [28] Darakananda, D., da Silva, A. F. C., Colonius, T., and Eldredge, J. D., "Data-Assimilated Low-Order Vortex Modeling of Separated Flows," *Physical Review Fluids*, Vol. 3, No. 12, 2018, Paper 124701. https://doi.org/10.1103/PhysRevFluids.3.124701
- [29] Milano, M., and Gharib, M., "Uncovering the Physics of Flapping Flat Plates with Artificial Evolution," *Journal of Fluid Mechanics*, Vol. 534, July 2005, pp. 403–409. https://doi.org/10.1017/S0022112005004842
- [30] Peng, D., and Milano, M., "Lift Generation with Optimal Elastic Pitching for a Flapping Plate," *Journal of Fluid Mechanics*, Vol. 717, Feb. 2013, p. R1. https://doi.org/10.1017/jfm.2012.614
- [31] An, X., Grimaud, L., and Williams, D. R., "Feedforward Control of Lift Hysteresis During Periodic and Random Pitching Maneuvers," *Active Flow and Combustion Control 2014*, edited by R. King, Springer International Publ., Cham, Switzerland, 2015, pp. 55–69.
- [32] Williams, D. R., An, X., Iliev, S., King, R., and Reißner, F., "Dynamic Hysteresis Control of Lift on a Pitching Wing," *Experiments in Fluids*, Vol. 56, No. 5, 2015, p. 112. https://doi.org/10.1007/s00348-015-1982-y
- [33] Williams, D. R., and King, R., "Alleviating Unsteady Aerodynamic Loads with Closed-Loop Flow Control," *AIAA Journal*, Vol. 56, No. 6, 2018, pp. 2194–2207. https://doi.org/10.2514/1.J056817
- [34] Xu, X., and Lagor, F. D., "Optimal Pitching in a Transverse Gust Encounter Using a Modified Goman-Khrabrov Model," AIAA Aviation 2021 Forum, AIAA Paper 2021-2937, 2021.
- [35] Lulekar, S. S., Ghassemi, P., Alsalih, H., and Chowdhury, S., "Adaptive-Fidelity Design Automation Framework to Explore Bioinspired Surface Riblets for Drag Reduction," *AIAA Journal*, Vol. 59, No. 3, 2021, pp. 880–892. https://doi.org/10.2514/1.J059613
- [36] Ahn, H.-S., Moore, K. L., and Chen, Y., Iterative Learning Control: Robustness and Monotonic Convergence for Interval Systems, Springer-Verlag, London, 2007, pp. 3–18.
- [37] Hjalmarsson, H., Gevers, M., Gunnarsson, S., and Lequin, O., "Iterative Feedback Tuning: Theory and Applications," *IEEE Control Systems Magazine*, Vol. 18, No. 4, 1998, pp. 26–41. https://doi.org/10.1109/37.710876
- [38] Sedky, G., Biler, H., and Jones, A. R., "Experimental Comparison of a Sinusoidal and Trapezoidal Transverse Gust," *AIAA Journal*, Vol. 60, No. 5, 2022, pp. 3347–3351. https://doi.org/10.2514/1.J061365
- [39] Goman, M., and Khrabrov, A., "State-Space Representation of Aero-dynamic Characteristics of an Aircraft at High Angles of Attack," *Journal of Aircraft*, Vol. 31, No. 5, 1994, pp. 1109–1115. https://doi.org/10.2514/3.46618
- [40] Greenblatt, D., Mueller-Vahl, H., Williams, D. R., and Reissner, F., "Goman-Khrabrov Model on a Pitching Airfoil with Flow Control," 8th AIAA Flow Control Conference, AIAA Paper 2016-4240, 2016. https://doi.org/10.2514/6.2016-4240
- [41] Williams, D. R., Reißner, F., Greenblatt, D., Müller-Vahl, H., and Strangfeld, C., "Modeling Lift Hysteresis on Pitching Airfoils with a Modified Goman–Khrabrov Model," *AIAA Journal*, Vol. 55, No. 2, 2017, pp. 403–409. https://doi.org/10.2514/1.J054937
- [42] Jacobs, E. N., and Sherman, A., "Airfoil Section Characteristics as Affected by Variations of the Reynolds Number," NACA-TR-586, Washington, Government Printing Office, 1939.
- [43] An, X., Williams, D. R., Eldredge, J. D., and Colonius, T., "Lift Coefficient Estimation for a Rapidly Pitching Airfoil," *Experiments in Fluids*, Vol. 62, No. 1, 2021, pp. 1–12. https://doi.org/10.1007/s00348-020-03105-3
- [44] Katz, J., and Plotkin, A., Low-Speed Aerodynamics, Vol. 13, Cambridge Univ. Press, Cambridge, England, U.K., 2001, Chap. 13.
- [45] Peters, D. A., Hsieh, M.-C. A., and Torrero, A., "A State-Space Airloads Theory for Flexible Airfoils," *Journal of the American Helicopter Society*, Vol. 52, No. 4, 2007, pp. 329–342.
- Society, Vol. 52, No. 4, 2007, pp. 329–342.
 [46] Brunton, S. L., and Rowley, C. W., "Empirical State-Space Representations for Theodorsen's Lift Model," *Journal of Fluids and Structures*, Vol. 38, April 2013, pp. 174–186. https://doi.org/10.1016/j.jfluidstructs.2012.10.005
- [47] Darwin, C., "Note on Hydrodynamics," Mathematical Proceedings of the Cambridge Philosophical Society, Vol. 49, No. 2, 1953, pp. 342–354. https://doi.org/10.1017/S0305004100028449

- [48] Stutz, C., Bohl, D. G., and Hrynuk, J. T., "Investigation of Lift Forces During Long Gust Interactions at Low Reynolds Number," AIAA Scitech 2022 Forum, AIAA Paper 2022-0042, 2022. https://doi.org/10.2514/6.2022-0042
- [49] Bryson, A. E., and Ho, Y.-C., *Applied Optimal Control: Optimization, Estimation, and Control*, Routledge, New York, 1975, Chap. 7.
- [50] Panton, R. L., Incompressible Flow, Wiley, Hoboken, NJ, 2006, Chap. 13.
- [51] Hemati, M. S., Eldredge, J. D., and Speyer, J. L., "Improving Vortex Models via Optimal Control Theory," *Journal of Fluids and Structures*,
- Vol. 49, Aug. 2014, pp. 91–111. https://doi.org/10.1016/j.jfluidstructs.2014.04.004
- [52] SureshBabu, A. V., Ramesh, K., and Gopalarathnam, A., "Model Reduction in Discrete-Vortex Methods for Unsteady Airfoil Flows," *AIAA Journal*, Vol. 57, No. 4, 2019, pp. 1409–1422. https://doi.org/10.2514/1.J057458

F. N. Coton Associate Editor